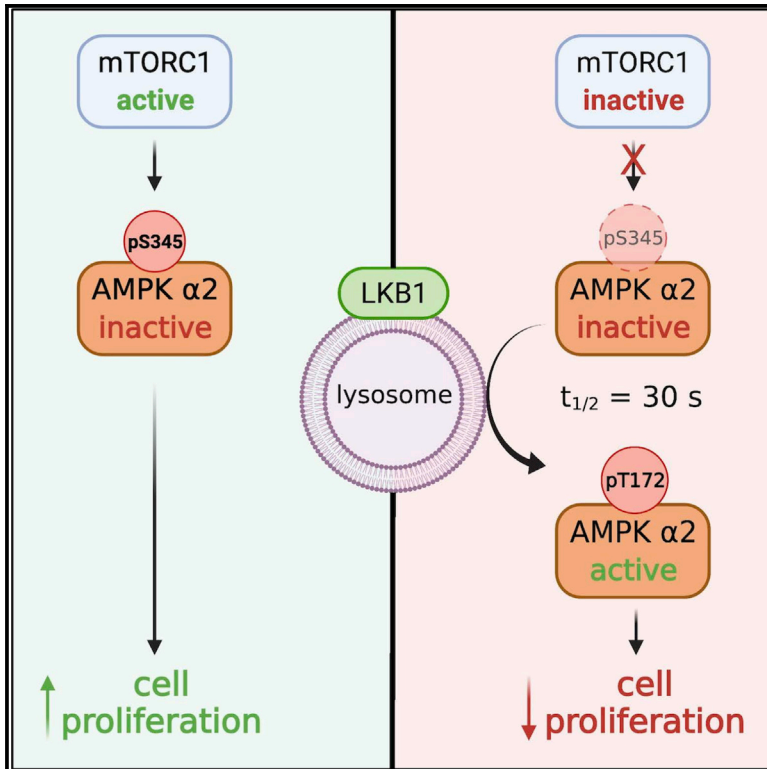


An AMPK α 2-specific phospho-switch controls lysosomal targeting for activation

Graphical abstract



Authors

Kaitlin R. Morrison, William J. Smiles, Naomi X.Y. Ling, ..., Bruce.E. Kemp, Janni Petersen, Jonathan S. Oakhill

Correspondence

janni.petersen@flinders.edu.au (J.P.), joakhill@svi.edu.au (J.S.O.)

In brief

Morrison et al. show that genetic loss or pharmacological suppression of AMPK α 2-S345 phosphorylation promotes accumulation of AMPK at lysosomes, a major cellular location for AMPK activation, and inhibits cell proliferation under nutrient stress conditions. Inhibiting AMPK α 2-S345 phosphorylation could be a therapeutic strategy to treat certain cancers.

Highlights

- Inhibitory phosphorylation of AMPK α 2-S345 is performed by multiple kinases
- Loss of α 2-S345 phosphorylation promotes AMPK accumulation at lysosomes
- AMPK residency at the lysosome is highly transient
- Endogenous α 2-S345A mutation suppresses cell proliferation under Arg/Leu stress



Article

An AMPK α 2-specific phospho-switch controls lysosomal targeting for activation

Kaitlin R. Morrison,^{1,7} William J. Smiles,^{2,7} Naomi X.Y. Ling,² Ashfaqu Hoque,² Gabrielle Shea,¹ Kevin R.W. Ngoei,³ Dingyi Yu,³ Lisa Murray-Segal,³ John W. Scott,^{3,4,5} Sandra Galic,³ Bruce.E. Kemp,^{3,4} Janni Petersen,^{1,6,*} and Jonathan S. Oakhill^{2,8,*}

¹Flinders Health and Medical Research Institute, Flinders University, Adelaide, SA 5042, Australia

²Metabolic Signalling Laboratory, St Vincent's Institute of Medical Research, School of Medicine, University of Melbourne, Melbourne, VIC 3065, Australia

³Protein Chemistry & Metabolism Unit, St Vincent's Institute of Medical Research, School of Medicine, University of Melbourne, Melbourne, VIC 3065, Australia

⁴Mary MacKillop Institute for Health Research, Australian Catholic University, Fitzroy, VIC 3000, Australia

⁵The Florey Institute of Neuroscience and Mental Health, Parkville, Melbourne, VIC 3052, Australia

⁶Nutrition and Metabolism, South Australia Health and Medical Research Institute, Adelaide, SA, Australia

⁷These authors contributed equally

⁸Lead contact

*Correspondence: janni.petersen@flinders.edu.au (J.P.), joakhill@svi.edu.au (J.S.O.)

<https://doi.org/10.1016/j.celrep.2022.110365>

SUMMARY

AMP-activated protein kinase (AMPK) and mechanistic target of rapamycin complex 1 (mTORC1) are metabolic kinases that co-ordinate nutrient supply with cell growth. AMPK negatively regulates mTORC1, and mTORC1 reciprocally phosphorylates S345/7 in both AMPK α -isoforms. We report that genetic or torin1-induced loss of α 2-S345 phosphorylation relieves suppression of AMPK signaling; however, the regulatory effect does not translate to α 1-S347 in HEK293T or MEF cells. Dephosphorylation of α 2-S345, but not α 1-S347, transiently targets AMPK to lysosomes, a cellular site for activation by LKB1. By mass spectrometry, we find that α 2-S345 is basally phosphorylated at 2.5-fold higher stoichiometry than α 1-S347 in HEK293T cells and, unlike α 1, phosphorylation is partially retained after prolonged mTORC1 inhibition. Loss of α 2-S345 phosphorylation in endogenous AMPK fails to sustain growth of MEFs under amino acid starvation conditions. These findings uncover an α 2-specific mechanism by which AMPK can be activated at lysosomes in the absence of changes in cellular energy.

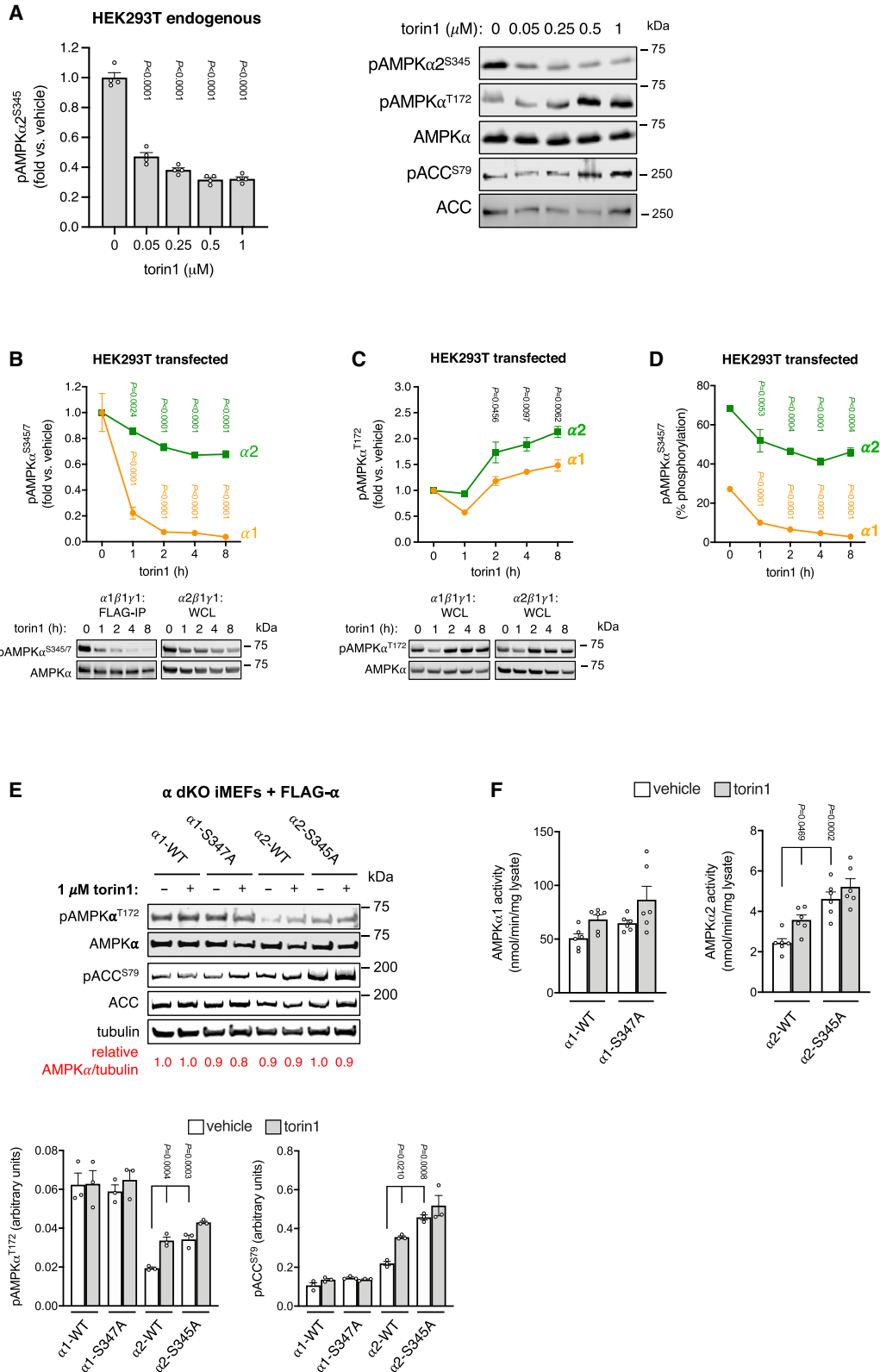
INTRODUCTION

Cell growth and proliferation are tightly controlled by the actions of two key regulators of metabolism, the mechanistic target of rapamycin (mTOR) and AMP-activated protein kinase (AMPK). mTOR is an atypical Ser/Thr protein kinase that forms the core catalytic component of at least two functionally and structurally distinct multi-protein complexes called mTORCs that are defined by unique regulatory partners (e.g., raptor, mTORC1; rictor, mTORC2) conferring substrate selectivity. mTORC1, originally defined by its sensitivity to the immunosuppressant drug rapamycin, integrates growth factor availability with cellular nutrient levels to drive anabolic (ATP-consuming) processes such as protein and lipid synthesis (Laplante and Sabatini, 2012). In contrast, AMPK is an $\alpha\beta\gamma$ heterotrimer expressed as several isoforms of a catalytic α -subunit (α 1/2) and regulatory β - (β 1/2) and γ -subunits (γ 1/2/3) that is activated in response to increases in intracellular AMP/ATP and ADP/ATP ratios; AMPK restores metabolic homeostasis by stimulating ATP- and nutrient-generating catabolic pathways such as autophagy (Oakhill et al., 2012; Garcia and Shaw, 2017). Canonical AMPK

activation in mammalian cells is triggered by exchange of ATP for AMP/ADP on the γ -subunit nucleotide-binding sites, resulting in α -subunit activation loop phosphorylation on T172 in the kinase domain. The principal α -T172 kinase involved in the metabolic stress response is liver kinase B1 (LKB1); however, AMPK is also phosphorylated on this residue in response to intracellular Ca^{2+} flux by the Ca^{2+} /calmodulin-dependent protein kinase, CaMKK2 (Oakhill et al., 2012). In addition, AMPK is phosphorylated on a disordered C-terminal Ser/Thr-rich region termed the "S/T-loop" [human α 1(472–525)] that overall serves to attenuate AMPK activity either by limiting phosphorylation of α -T172 (α -S487/491 [Horman et al., 2006; Hurley et al., 2006; Hawley et al., 2014; Heathcote et al., 2016; Dagon et al., 2012; Coughlan et al., 2016]) or promoting its dephosphorylation (α -T479 [Suzuki et al., 2013]). This poorly conserved region accounts for the greatest degree of sequence divergence between α isoforms, indicative of why such a broad array of physiological stimuli and regulatory kinases modulate these sites.

We recently found that mTORC1 directly phosphorylates AMPK on an evolutionarily conserved residue S367 in the fission yeast AMPK catalytic subunit Ssp2, and on the equivalent





(legend on next page)

mammalian AMPK α 1-S347 and α 2-S345 sites, that was associated with reduced Ssp2 and α 2AMPK activity (Ling et al., 2020). As such, our work defined an ancestral negative feedback loop between these two nutrient-sensing enzymes (Ling et al., 2020; Gwinn et al., 2008). An emerging point of interest in the field relates to the cellular location where AMPK activity is governed. α -T172 phosphorylation by LKB1 has been reported to occur on the surface of late endosomes/lysosomes, mediated by formation of an axin1 scaffold consisting of AMPK and LKB1 docking onto the resident lysosomal protein complex v-ATPase-Ragulator (Zhang et al., 2014). The v-ATPase-Ragulator complex has been well-characterized as a platform responsible for tethering mTORC1 to the lysosomal surface in response to amino acid stimulation, where it is directly activated by the small GTPase Rheb (Zoncu et al., 2011; Inoki et al., 2003; Sancak et al., 2008; Menon et al., 2014). Nearly 20 years ago, AMPK was found to be N-terminally myristoylated on Gly2 of its β -subunit (Warden et al., 2001), which we later revealed afforded endogenous membrane association (Oakhill et al., 2010). Notably, this co-translational modification is required for AMPK targeting to lysosomes in response to glucose starvation (Zhang et al., 2017). Until now, there has been a paucity of information pertaining to how post-translational modifications regulate subcellular trafficking of AMPK; we recently showed that phosphorylation of the γ 1-subunit (residues S192 and T284) by another atypical protein kinase, DNA-PK, promoted its lysosomal localization and association with LKB1 in response to glucose starvation (Puustinen et al., 2020). Here, we further investigated α -isoform-specific regulatory effects of the S345/S347 phosphorylation site. We found that relieving phosphorylation of this site targets α 2-AMPK, but not α 1-AMPK, to the lysosome. Consistent with our previous findings using AMPK overexpression systems, loss of α 2-S345 phosphorylation in endogenous AMPK in MEFs was associated with stunted cell proliferation under conditions of amino acid starvation.

RESULTS

Differential regulation of AMPK α isoforms by mTORC1

We previously demonstrated that downregulation of mTORC1 in immortalized mouse embryonic fibroblasts (iMEFs) by the allosteric inhibitor rapamycin, ATP-competitive inhibitor torin1, or

the mitochondrial complex I inhibitor phenformin caused near-complete loss of phosphorylation of α 1-S347 (α 1-pS347) but only partial loss of α 2-pS345 after 2 h (Ling et al., 2020). Using an α 2-pS345 phosphospecific antibody, we confirmed that endogenous α 2-pS345 in the highly proliferative human cell line HEK293T was reduced in a torin1 dose-dependent manner but was retained at \sim 30% basal level even after 8-h incubation with 1 μ M torin1, the maximal cellular dose reported to avoid off-target effects (Liu et al., 2012) (Figure 1A). This was accompanied by dose-dependent increases in T172 phosphorylation and AMPK signaling, as measured by phosphorylation of S79 on acetyl-CoA carboxylase (ACC). Because of limitations associated with using our α 1-pS347 phosphospecific antibody to probe whole cell lysates, we tracked pS345/347 in HEK293T cells transfected to overexpress FLAG-tagged α 1 β 1 γ 1 or α 2 β 1 γ 1 AMPK heterotrimers (Figure 1B). Incubation of these cells with 250 nM torin1 led to near-complete reduction of pS347 on FLAG-immunoprecipitated α 1-AMPK within 2 h, whereas \sim 70% of the basal α 2-S345 signal was retained even after 8 h. Torin1 significantly augmented α 2-pT172 after 2 h, at which time point phosphorylation of α 1-T172 was no different from basal, albeit recovering from an initial decrease at 1 h we consider may be due to regulation of other AMPK phosphorylation sites (Figure 1C) (Puustinen et al., 2020). This preferential α 2 activation persisted throughout the remaining duration of the 8-h time course.

We next used mass spectrometry to verify the phosphorylation stoichiometries of α -S345/7, both basally and in response to torin1. FLAG-immunoprecipitated AMPK was digested and tryptic peptides were subjected to tandem mass spectrometry for precise detection of phosphorylation stoichiometries (percentage of phospho-peptide) (Steen et al., 2005). α 2-S345 was found to be abundantly phosphorylated during high nutrient conditions conducive to mTORC1 activity, whereas S347-phosphorylated species represented a much smaller fraction of total α 1-AMPK (α 2: 68% phosphorylation; α 1: 27% phosphorylation) (Figure 1D). Consistent with immunoblotting, α 1-pS347 was markedly reduced by torin1 at 1 h, with the signal attenuated by almost 90% after 8 h. The rate of α 2-pS345 dephosphorylation and absolute change in pS345 stoichiometry were similar by comparison; however, in contrast to α 1, α 2-pS345 dephosphorylation bottomed out at 40% to 50% stoichiometry,

Figure 1. mTORC1-mediated inhibition of AMPK is restricted to α 2-containing complexes

(A) HEK293T cells were treated with (0–1 μ M) rapamycin or torin1 for 8 h and harvested lysates immunoblotted for AMPK α 2-pS345. Data are shown as mean phosphorylation (arbitrary units) \pm SEM; n = 4. Statistical significance versus vehicle was calculated by one-way ANOVA with Dunnett's multiple-comparisons test. HEK293T cells, transiently expressing either FLAG-tagged α 1 β 1 γ 1 or α 2 β 1 γ 1, were incubated with 250 nM torin1 for up to 8 h. (B–D) Harvested lysates were (B) immunoblotted for AMPK α -pS345/347 (α 1 β 1 γ 1 was purified on FLAG agarose beforehand to exclude a nonspecific band migrating at \sim 60 kDa), (C) immunoblotted for AMPK α -pT172, or (D) prepared for quantitative tandem mass spectrometry (MS/MS) analysis. For (B) and (C), data are shown as mean fold change in phosphorylation versus vehicle \pm SEM; n = 4. For (D), data are shown as mean % phosphorylation \pm SEM; n = 4. For (B) and (D), statistical significance versus vehicle was calculated by one-way ANOVA with Dunnett's multiple-comparisons test. For (C), statistical significance versus α 1-pT172 for each time point was calculated by two-tailed Student's t test. (E) α dKO iMEFs expressing FLAG-tagged α 1 (WT or S347A) or α 2 (WT or S345A) were treated with 1 μ M torin1 for 120 min and harvested lysates immunoblotted as indicated. Data are shown as mean phosphorylation (arbitrary units) \pm SEM; n = 3. Statistical significance versus vehicle-treated WT was calculated by one-way ANOVA with Dunnett's multiple-comparisons test. (F) AMPK complexes from similarly treated cells were immobilized on FLAG agarose and assayed for activity. Data are shown as mean AMPK activity (nmol min⁻¹ mg⁻¹) \pm SEM; n = 6. Statistical significance versus vehicle-treated WT was calculated by one-way ANOVA with Dunnett's multiple-comparisons test. Representative immunoblots are shown. All phospho- and total protein signals were detected on the same membrane except (B), for which α 2-pS345 and total α 2 were immunoblotted on separate membranes from the same lysate preparation. n corresponds to the number of independent biological experiments.

indicating that a significant level of $\alpha 2$ -S345 phosphorylation was retained in the presence of torin1.

To further explore AMPK isoform-specific regulation by mTORC1, we tested whether dephosphorylation of $\alpha 1$ -pS347 recapitulates the biochemical and cellular effects observed for $\alpha 2$ -pS345 dephosphorylation (Ling et al., 2020). We expressed FLAG epitope-tagged human AMPK $\alpha 1$ or $\alpha 2$ subunits in AMPK $\alpha 1/\alpha 2$ (*Prkaa1*^{-/-}; *Prkaa2*^{-/-})-double-knockout immortalized mouse embryonic fibroblasts (α dKO iMEFs) by lentiviral-mediated delivery to reconstitute the AMPK heterotrimer at consistent levels (Dite et al., 2017), and assessed activity and downstream signaling in response to torin1. Torin1 efficacy was confirmed by dephosphorylation of canonical mTORC1 substrates unc-51-like kinase 1 (ULK1) S757 and eIF4E-binding protein 1 (4E-BP1)-T37/46 (Figure S1A), whereas signaling was assessed by phosphorylation of AMPK substrates ACC-S79 and ULK1-S555. In $\alpha 2$ -expressing dKO iMEFs, pT172, pACC-S79, and AMPK activity was significantly augmented by exposure to torin1, as previously reported (Figures 1E and 1F). Similar increases in these parameters, and increased ULK1-pS555, were induced by expression of the $\alpha 2$ -S345A mutant, which were refractory to further stimulation by torin1 (Figures 1E and S1B). Torin1 lowered ULK1-pS555 in both cell lines (Figure S1B), an effect previously observed with rapamycin and the ATP-competitive mTOR inhibitor pp242 (Gordeev et al., 2015). Conversely, both torin1 treatment of $\alpha 1$ -expressing dKO iMEFs, or expression of $\alpha 1$ -S347A mutant, failed to elicit any significant increases in pT172, AMPK activity or downstream signaling (Figures 1E and 1F and S1B). Interestingly, $\alpha 2$ -expressing iMEFs displayed substantially reduced basal T172 phosphorylation and AMPK activity compared with $\alpha 1$ cells, yet ACC signaling was elevated (Figures 1E and 1F). This observation hints at some degree of α isoform-specific signaling, with one interpretation being that $\alpha 2$ -AMPK more efficiently regulates ACC in these cells than $\alpha 1$.

mTORC1 substrates have previously been categorized as either “good” or “bad” depending on their sensitivity to rapamycin, a partial inhibitor of mTORC1 signaling. Good mTORC1 substrates, such as 4E-BP1-T37/46 and ULK1-S757, remain phosphorylated in cells treated with rapamycin, while weaker or bad substrates, like p70 ribosomal S6 kinase (p70S6K)-T389, are rapidly dephosphorylated (Kang et al., 2013; Thoreen et al., 2009). To grade α -S345/347 as mTORC1 substrates, HEK293Ts expressing FLAG-tagged $\alpha 1\beta 1\gamma 1$ or $\alpha 2\beta 1\gamma 1$ were treated with 250 nM rapamycin (the maximal amount at which rapamycin-sensitive substrates are dephosphorylated [Kang et al., 2013]) or torin1 for 24 h, with α -pS345/7 analyzed by immunoblotting alongside canonical mTORC1 substrates. Regardless of overexpression of $\alpha 1$ or $\alpha 2$, ULK1-pS757 and 4E-BP1-pT37/46 retained their resistance to rapamycin, whereas marked p70S6K-pT389 dephosphorylation occurred by 5 min with each inhibitor (Figure S1C). Incubation with rapamycin or torin1 resulted in significant dephosphorylation of $\alpha 1$ -pS347 after 5 min; however, resistance to rapamycin, relative to torin1, was observed at all time points from 30 min until the $\alpha 1$ -pS347 signal had already reached negligible levels with torin1 (Figure S1D). $\alpha 2$ -pS345 was significantly decreased by rapamycin after 30 min, and 4-h exposure was required to detect a significant decrease in dephosphorylation of $\alpha 2$ -pS345 by torin1 relative to rapamycin. It should be

noted that interpretation of the dephosphorylation rates of $\alpha 2$ -pS345 was confounded to some extent by the inability of either inhibitor to elicit complete $\alpha 2$ -pS345 dephosphorylation (rapamycin: maximum $\sim 30\%$ decrease in basal signal; torin1: maximum $\sim 40\%$ decrease in basal signal). Thus, we are unable to classify $\alpha 1$ -S347 and $\alpha 2$ -S345 as either good or bad mTORC1 substrates, with both representing an intermediate class of mTORC1 targeting. Combined, these data indicate that while mTORC1 phosphorylates both α isoforms at the S345/7 site, inhibitory regulation of AMPK through this site is exclusive to $\alpha 2$ in these cell lines. The inability of torin1 to induce complete dephosphorylation of $\alpha 2$ -pS345 also strongly indicates the likelihood of an alternate, $\alpha 2$ -specific kinase(s) regulating this site.

GSK3 regulates phosphorylation of fission yeast Ssp2-S367 and phosphorylates purified mammalian AMPK α -S345/7

To search for alternate kinase(s) regulating α -pS345/7, we screened a fission yeast *Schizosaccharomyces pombe* kinase deletion library (Bimbo et al., 2005) in the presence of torin1 to abrogate the TORC1-dependent phosphorylation of Ssp2-S367 (equivalent of mammalian AMPK α -S345/7). Glycogen synthase kinase (GSK3) was identified as a potential candidate, since Ssp2-pS367 was significantly reduced in a *gsk3* deletion strain (Figure 2A). Notably, GSK3, in particular the β isoform, has been shown to phosphorylate mTORC1 substrates such as 4E-BP1 and p70S6K, inducing similar effects on cell growth and proliferation (Shin et al., 2011, 2014). Both sequences surrounding Ssp2-S367 and α -S345/7 sites contain elements of a GSK3 β consensus motif (Hornbeck et al., 2015) (Figure 2B). Using purified enzymes *in vitro*, we found that GSK3 β phosphorylated α -S345/7 on kinase-inactive $\alpha 1$ (D139A) $\beta 1\gamma 1$ and $\alpha 2$ (D141A) $\beta 1\gamma 1$ (Figure 2C). However, we could not validate $\alpha 2$ -S345 as a GSK3 β substrate in HEK293T cells (Figure 2D), whereby treatment with CT99021, a potent, ATP-competitive inhibitor of GSK3 (Bain et al., 2007), failed to have any effect on endogenous $\alpha 2$ -pS345, either in isolation or when co-incubated with torin1. CT99021 efficacy was apparent in HEK293Ts as indexed by suppressed phosphorylation of another GSK3 target site on AMPK, $\alpha 1$ -T479 (Suzuki et al., 2013), as well as S641 on glycogen synthase (Figure 2D). Since GSK3 regulation of AMPK may be enhanced by serum starvation (Suzuki et al., 2013), we repeated the same treatments following overnight serum deprivation of HEK293Ts. Under these conditions, CT99021 failed to elicit a significant reduction in $\alpha 2$ -pS345, and in contrast to findings in fission yeast, it did not potentiate the torin1-induced loss of $\alpha 2$ -pS345 (Figure 2E). Thus, unlike mTORC1, GSK3 is not a major $\alpha 2$ -S345 kinase in asynchronously dividing HEK293T cells, at least under the conditions tested. Future studies are required to identify mammalian $\alpha 2$ -S345 kinases besides mTORC1.

$\alpha 2$ -S345 phosphorylation regulates AMPK trafficking to lysosomes

We next wanted to determine which of the upstream kinases, LKB1 or CaMKK2, was responsible for activating AMPK in response to $\alpha 2$ -pS345 dephosphorylation. To address this, we used HeLa cells, which are devoid of LKB1 expression. Unlike the effect in iMEFs (Figure 1E), neither incubation with torin1

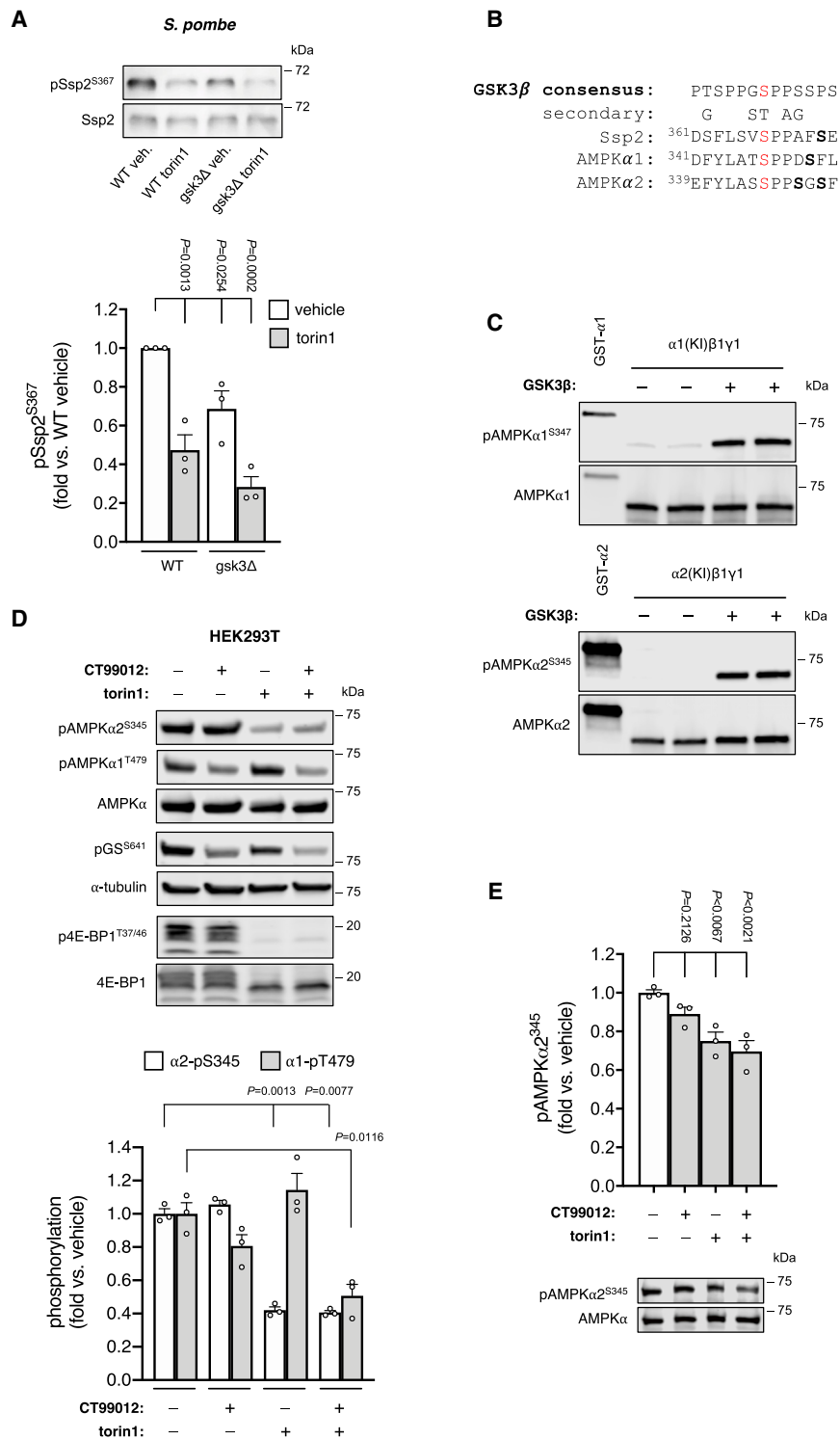


Figure 2. GSK3 regulates Ssp2-S367 in *S. pombe*, but not the equivalent AMPK α -S345/S347 phosphorylation sites in HEK293T cells

(A) *S. pombe* strains (WT and GSK3 β deleted [gsk3 Δ]) were incubated \pm 25 μ M torin1 for 2 h and harvested lysates immunoblotted as indicated. Data are shown as mean fold change in Ssp2-pS367 versus vehicle \pm SEM; n = 3. Statistical significance versus vehicle or torin1 treated WT was calculated by one-way ANOVA with Dunnett's multiple-comparisons test.

(B) Alignment of the primary sequence surrounding *S. pombe* Ssp2-S367 (in red) and conserved residues in mammalian AMPK α 1 and α 2. The GSK3 β consensus sequence and secondary preferences are shown above (www.phosphosite.org), and possible phosphorylation priming sites in Ssp2 and AMPK α 1/2 at P+3, 4 and 5 are highlighted in bold. Alignment was generated by ClustalX.

(C) GSK3 β phosphorylates AMPK α -S345/7 *in vitro*. Purified, kinase-inactive, His-tagged α 1 β 1 γ 1 (left) or α 2 β 1 γ 1 (right) was incubated \pm GSK3 β and MgATP for 30 min at 30°C and immunoblotted as indicated. GST-tagged α 1 β 1 γ 1 and α 2 β 1 γ 1 AMPK, expressed in HEK293T cells, were used as respective positive controls.

(D) HEK293T cells were incubated with inhibitors CT99012 (GSK3 β) and/or torin1 (mTORC) for 8 h and harvested lysates immunoblotted as indicated. Data are shown as mean fold change in phosphorylation versus vehicle \pm SEM; n = 3. Statistical significance versus vehicle was calculated by one-way ANOVA with Dunnett's multiple-comparisons test.

(E) HEK293T cells were serum starved overnight prior to incubation with CT99012 and/or torin1 for 120 min and harvested lysates immunoblotted as indicated. Data are shown as mean fold change in phosphorylation versus vehicle \pm SEM; n = 3. Statistical significance versus vehicle was calculated by one-way ANOVA with Dunnett's multiple-comparisons test. n corresponds to the number of independent biological experiments. Representative immunoblots are shown.

results point to LKB1 being the AMPK-activating kinase in response to α 2-pS345 dephosphorylation; however, this has yet to be demonstrated conclusively.

We (Puustinen et al., 2020) and others (Zhang et al., 2014, 2017) have described the external surface of the lysosomal membrane as a major cellular activating hub for AMPK by LKB1. Using an established and rapid immunoprecipitation (IP) protocol (Abu-Remaileh et al., 2017) to isolate lyso-

some from iMEF cells stably expressing an HA-tagged lysosomal transmembrane protein TMEM192, we confirmed significantly enhanced α -T172 phosphorylation in this fraction compared with whole cell lysates (Figure 3B). Confidence in the purity of the lysosomal isolation method was evidenced by AMPK

nor expression of the α 2-S345A mutation resulted in elevated pT172 of GFP- α 2 β 1 γ 1 transiently expressed in HeLa cells (Figure 3A). Notably, these effects were despite wild-type (WT) α 2 and α 2-S345A complexes retaining sensitivity, as denoted by increased α -pT172, to the CaMKK2 activator ionomycin. These

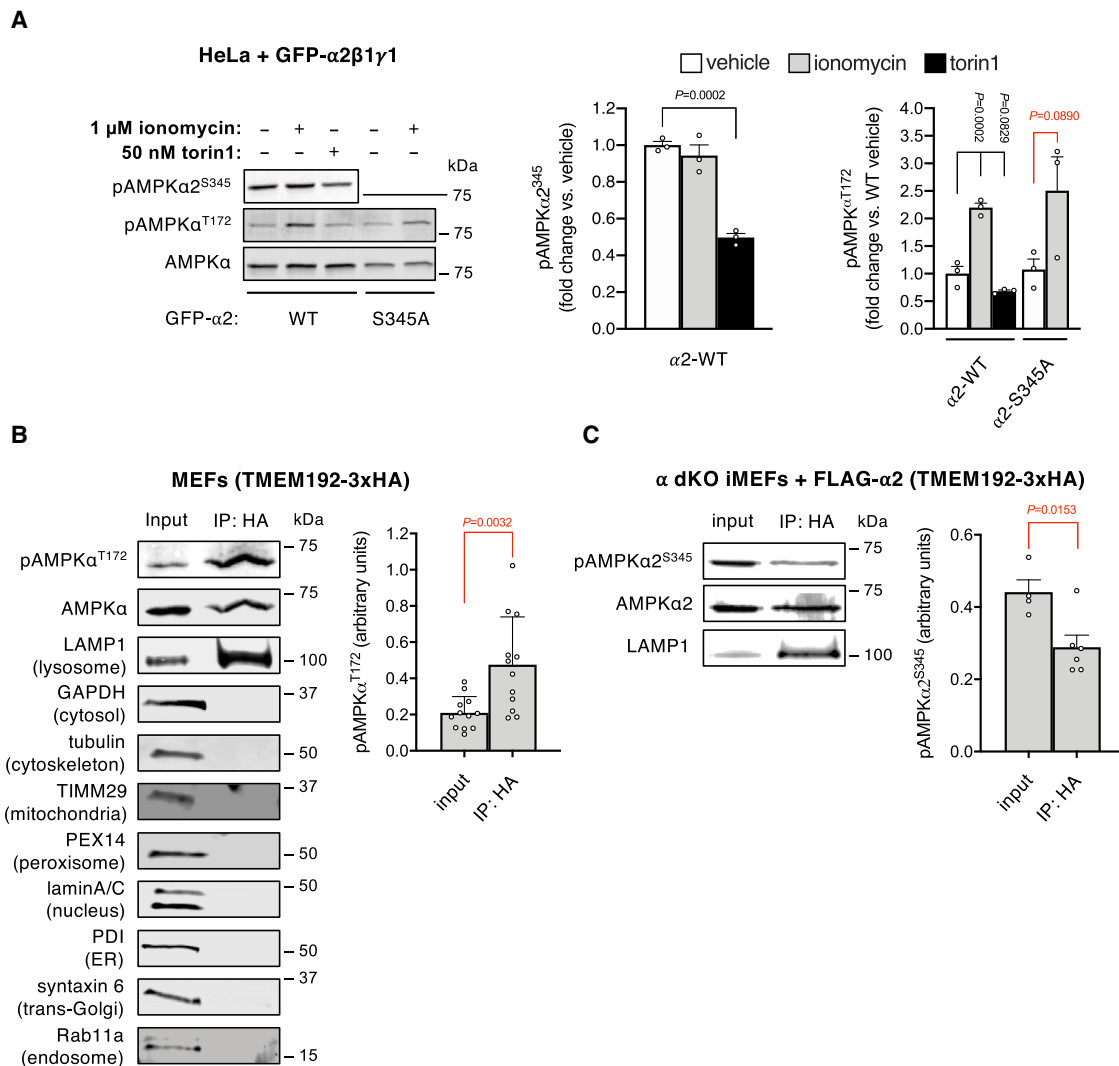


Figure 3. $\alpha 2$ -S345 phosphorylation inhibits AMPK activation by LKB1

(A) HeLa cells, transiently expressing GFP-tagged $\alpha 2\beta 1\gamma 1$ (WT and $\alpha 2$ -S345A mutant), were treated with 1 μ M ionomycin or 50 nM torin1 for 5 min and 60 min, respectively, and immunoblotted for $\alpha 2$ -pS345 and α -pT172. Data are shown as mean fold change in phosphorylation versus vehicle \pm SEM; n = 3. Statistical significance versus vehicle-treated cells expressing WT AMPK was calculated by one-way ANOVA with Dunnett's multiple-comparisons test, or versus vehicle-treated cells expressing $\alpha 2$ -S345A AMPK by two-tailed Student's t test (red p value).

(B) Lysates (input) were prepared from iMEFs stably expressing the integral lysosomal membrane protein TMEM192-3xHA. Lysosomes were rapidly immunoprecipitated on HA-agarose and immunoblotted for α -pT172, and markers for cellular compartments as indicated. Data are shown as mean pT172/ α (arbitrary units) \pm SEM; n = 12. Statistical significance versus input was calculated by two-tailed Student's t test.

(C) Lysates (input) were prepared from α dKO iMEFs expressing FLAG-tagged $\alpha 2$ and TMEM192-3xHA. Lysosomes were rapidly immunoprecipitated on HA-agarose and immunoblotted for $\alpha 2$ -pS345. Data are shown as mean $\alpha 2$ -pS345/ α (arbitrary units) \pm SEM; n = 4. Statistical significance versus input was calculated by two-tailed Student's t test. n corresponds to the number of independent biological experiments. Representative immunoblots are shown.

coprecipitating exclusively with LAMP1 (another transmembrane lysosomal protein) and not with any other markers of cellular membrane-bound organelles or compartments. Notably, the AMPK pool enriched in lysosomal fractions possessed significantly reduced $\alpha 2$ -pS345 compared with AMPK in whole cell material, despite basal lysosomal IP experiments being carried out in complete cell culture media (Figure 3C).

To investigate the link between $\alpha 2$ -pS345 status and lysosome trafficking, we transiently expressed GFP- $\alpha 2\beta 1\gamma 1$ in

HeLa cells and tracked cellular localization using fluorescent microscopy. Live-cell imaging experiments confirmed that WT GFP- $\alpha 2$ and the glutamic acid $\alpha 2$ -S345E phosphomimetic substitution adopt a predominantly cytosolic distribution (Figure S2). In contrast, GFP signals associated with the $\alpha 2$ -S345A mutant in cells grown in complete media, or WT $\alpha 2$ in cells acutely starved of glucose for 20 min, both overlapped with FM4-64, a marker of endocytic membranes (Figure S2). In addition, fixed cells stained for the lysosomal

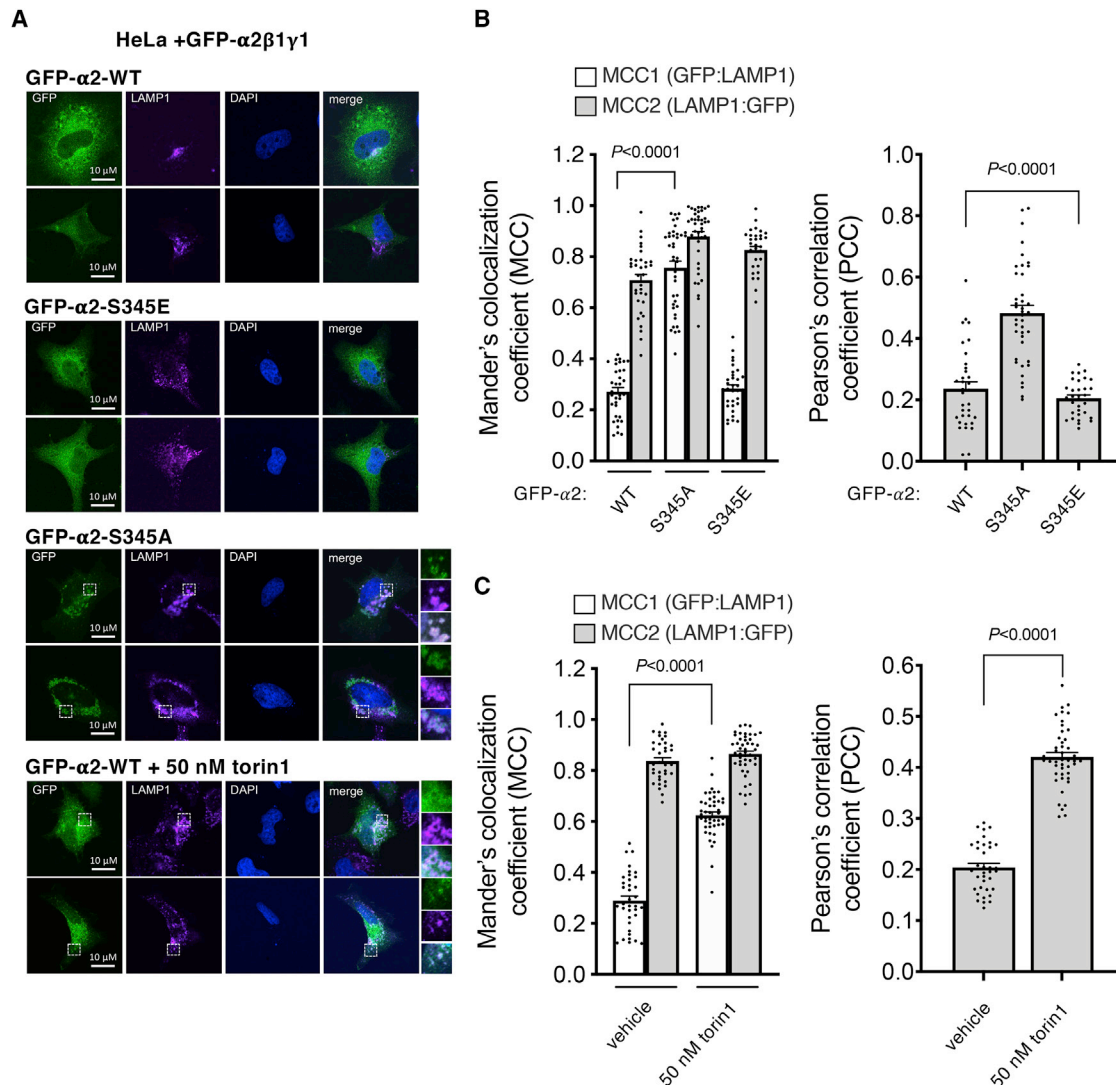


Figure 4. $\alpha 2$ -S345 phosphorylation attenuates AMPK localization to lysosomes

(A) Representative confocal microscopy images of HeLa cells transiently expressing GFP-tagged $\alpha 2\beta 1\gamma 1$ (WT, $\alpha 2$ -S345E and $\alpha 2$ -S345A mutants, or WT treated with 50 nM torin1 for 1 h). Cells were stained with DAPI (blue, nuclei) and anti-LAMP1 antibody (purple, lysosomes). Individual images (shown below merged images) were collected using identical settings.

(B and C) Image analyses (WT; n = 34–36, $\alpha 2$ -S345E; n = 32, $\alpha 2$ -S345A; n = 40; WT + torin1; n = 46) are presented as mean Mander's colocalization coefficient \pm SEM (MCC, a measure of the fraction of one protein that colocalizes with another: MCC1 – fraction of GFP signal colocalized with LAMP1 signal; MCC2 – fraction of LAMP1 signal colocalized with GFP signal), and mean Pearson's correlation coefficient \pm SEM (PCC, a measure of the relationship between signal intensities) for (B) $\alpha 2$ -S345A and $\alpha 2$ -S345E, and (C) torin1 treatment compared with WT and untreated. For (B), statistical significance versus cells expressing WT AMPK was calculated by one-way ANOVA with Dunnett's multiple-comparisons test. For (C), statistical significance versus vehicle-treated cells was calculated by one-way ANOVA with Dunnett's multiple-comparisons test.

marker LAMP1 revealed that the $\alpha 2$ -S345A mutant displays increased colocalization and correlation with LAMP1 by ~ 2.5 -fold relative to WT $\alpha 2$ and the $\alpha 2$ -S345E mutant (Figures 4A and 4B). Fluorescence recovery after photo bleaching (FRAP) of GFP- $\alpha 2$ S345A-expressing HeLa cells was recovered to 50% within 30 s of bleaching (Figure 5), highly reminiscent of the resident time of mTORC1 on lysosomes (Manifava et al., 2016). One-hour torin1 treatment of GFP- $\alpha 2$ -expressing cells also increased AMPK lysosomal translocation (Figures 4A and 4C) to a similar degree previously reported in

HEK293 cells in response to glucose starvation (Zhang et al., 2017). In contrast, there were no differences in colocalization and correlation with LAMP1 of $\alpha 1$ WT and $\alpha 1$ -S347A/E mutants, with all AMPK complexes primarily dispersed throughout the cytosol (Figure S3).

A proposed mechanism of lysosomal targeting is the binding of AMPK with the molecular scaffold axin1, that then tethers to the resident lysosomal v-ATPase-Ragulator complex to facilitate LKB1 phosphorylation on α -T172 (Zhang et al., 2014). Since glucose starvation has been reported to elicit this interaction

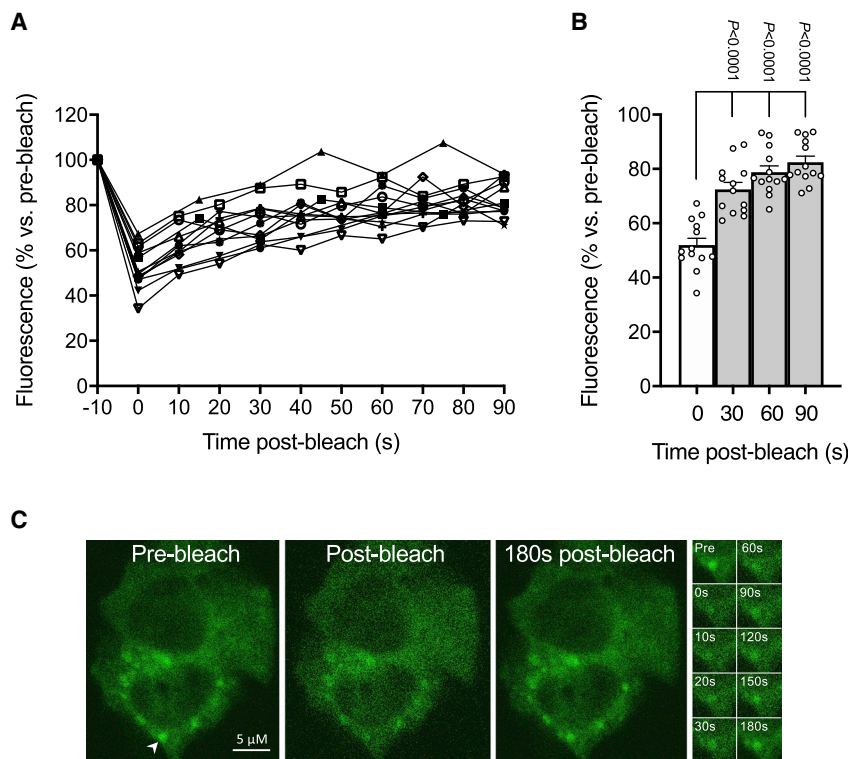


Figure 5. AMPK residency on lysosomal membranes is transient

(A and B) FRAP was performed on HeLa cells, transiently expressing GFP-tagged $\alpha 2$ -S345A $\beta 1\gamma 1$, on a Leica Laser Scanning Confocal Microscope. Images were taken pre-bleached, followed by successive post-bleached images for up to 3 min. Data are shown as mean fluorescence (relative to pre-bleached) \pm SEM, $n = 13$ cells from five independent transfections. Statistical significance versus pre-bleach was calculated by one-way ANOVA with Dunnett's multiple-comparisons test. (C) Representative images.

(Zhang et al., 2017) and inhibit mTORC1 to promote $\alpha 2$ -pS345 dephosphorylation (Ling et al., 2020), we glucose-deprived α dKO iMEFs reconstituted with FLAG- $\alpha 1$ or - $\alpha 2$ and analyzed FLAG-immunoprecipitated material. Despite appreciable cellular axin1 expression and strict adherence to a protocol purported to preserve AMPK/axin1 interactions (Zhang et al., 2018), we did not detect coimmunoprecipitation of axin1 with either $\alpha 1$ - or $\alpha 2$ -AMPK, regardless of the cellular nutrient state (Figure S4). Therefore, we are unable to confirm a requirement for AMPK/axin1 binding to the v-ATPase-Ragulator as a mechanism for lysosomal targeting and activation of AMPK following mTORC1 inhibition.

Combined, our data indicate that localization of $\alpha 2$ -AMPK at the lysosome, an event previously associated with activation by LKB1, is negatively regulated by mTORC1-mediated phosphorylation of $\alpha 2$ -S345, via a mechanism independent of tethering to axin1. We did not observe a similar regulatory role for $\alpha 1$ -pS347, possibly explaining why dephosphorylation of this site in the absence of nutrient stress is insufficient to trigger significant increases in AMPK activity. AMPK tethering to the lysosome is also transient and highly dynamic, indicating continual replenishment of the AMPK pool at lysosomal surfaces.

α -pS345/7 dephosphorylation delays cell proliferation

Previously, real-time analysis of proliferation by live-cell imaging in the Incucyte system indicated that phosphorylation of $\alpha 2$ -S345 promotes cell proliferation in response to energy stress that stimulates autophagy (Ling et al., 2020). Since these results were obtained using an AMPK overexpression

system, we generated an $\alpha 2$ -S345A knockin mouse by CRISPR technology (Figure S5). We found that rates of cell proliferation were not significantly altered between MEFs derived from WT or $\alpha 2$ -S345A knockin mice in complete media (25 mM glucose); however, proliferation of $\alpha 2$ -S345A MEFs was significantly attenuated at 40 h or beyond, relative to WT, in amino acid (arginine, leucine, or arginine and leucine) deprived media (Figure 6). These results confirm, in an endogenous AMPK setting, our previous conclusion that mTORC1-induced phosphorylation of $\alpha 2$ -S345 constrains AMPK activity to facilitate cell proliferation under nutrient stress.

DISCUSSION

AMPK $\alpha 2$ -S345 is an evolutionarily conserved substrate for mTORC1 that suppresses AMPK signaling without affecting allosteric regulation by AMP. Instead, here we report that dephosphorylation of $\alpha 2$ -pS345 promotes targeting to lysosomes, where AMPK has been reported to be phosphorylated on the activation loop residue α -T172 by LKB1 in response to energy stress (Zhang et al., 2014, 2017). In agreement with these findings, acutely starving mammalian cells of glucose induces enrichment of $\alpha 2$ -containing AMPK complexes on organelles of the endocytic pathway. These organelles were confirmed to be lysosomes by genetic and pharmacologic methods in fixed cells. In addition, even under basal conditions, a proportion of AMPK presenting with attenuated $\alpha 2$ -S345 phosphorylation is localized to the lysosome. Because mTORC1 inhibitors have no acute bearing on the cellular adenylate charge (Ling et al., 2020; Dite et al., 2017), dephosphorylation of AMPK $\alpha 2$ -S345 alone, even in the presence of adequate nutrients, is sufficient to both direct AMPK to the lysosome and elicit AMPK activation.

Divergent forms of energy stress, such as glucose starvation that attenuates mTORC1 signaling, are thought to promote AMPK trafficking to the lysosome for activation via axin and v-ATPase-Ragulator scaffolding in cell lines (MEFs, HEK293Ts) largely expressing the $\alpha 1$ isoform (Zhang et al., 2014, 2017). However, this mechanism of AMPK activation could not be independently corroborated using HEK293T cells in a recent study

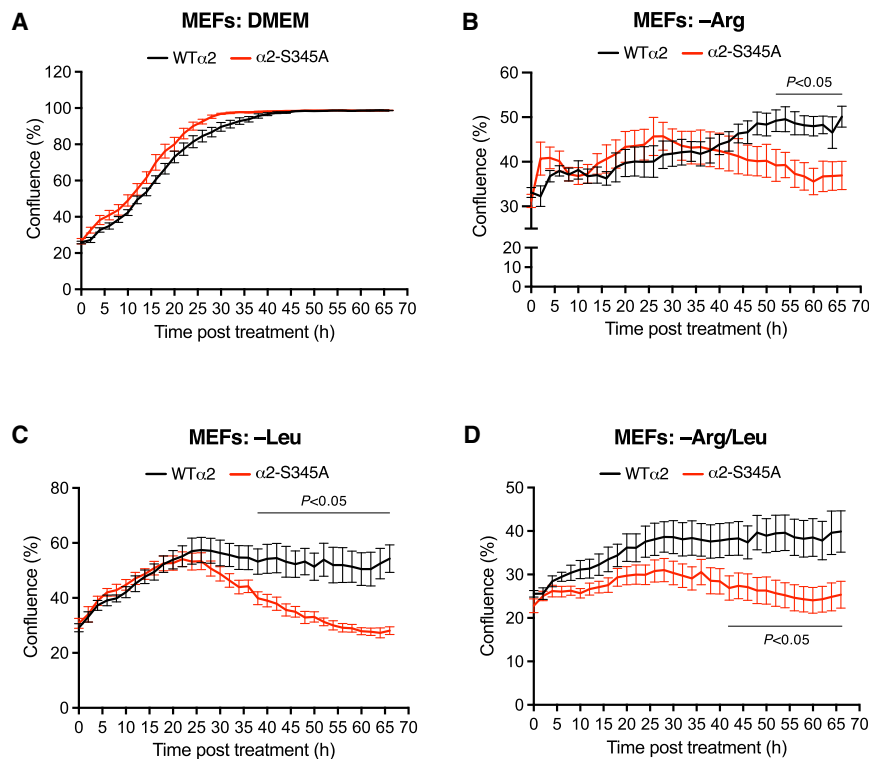


Figure 6. Loss of α 2-S345 phosphorylation reduces proliferation rates of MEF cells under conditions of nutrient stress

(A–D) AMPK WT or α 2-S345A MEFs were identically seeded in full DMEM. At 20% to 30% confluence, media was replaced with (A) full DMEM, (B) DMEM deficient in arginine, (C) DMEM deficient in leucine, or (D) DMEM deficient in arginine and leucine, and cell proliferation tracked in an Incucyte live-cell imaging system. Data shown as mean % confluence, \pm SEM; $n = 6$ –9. Statistical significance versus WT at each time point was calculated by unpaired t test. n corresponds to the number of independent biological experiments.

investigating mTORC1 activation by glucose (Orozco et al., 2020), and we too were unable to identify AMPK/axin1 binding in iMEF cells, regardless of the α isoform, in response to glucose starvation. Moreover, in one study (Zhang et al., 2014), pharmacologic (rapamycin or torin1) inhibition of mTORC1 alone, or in combination with glucose starvation, failed to enhance AMPK activation and downstream signaling. While we did find that isolated lysosomes copurified with an active pool of AMPK in iMEFs, which predominantly express the α 1 isoform, dephosphorylation of α 1-pS347, unlike α 2-pS345, was inconsequential in terms of promoting AMPK lysosomal enrichment, activity, and signaling when cells were cultured in complete media. Therefore, mTORC1-regulated lysosomal targeting and activation of AMPK favors α 2-containing heterotrimers in HEK293T and MEF cells.

Lysosomal targeting and activation of AMPK is a rapid process (less than 1 min), reminiscent of the dynamics of mTORC1 lysosome-to-cytoplasm exchange rates under nutrient-replete conditions (Lawrence et al., 2018). When nutrients are in abundance, the v-ATPase-Ragulator complex harnesses mTORC1 at the lysosomal surface, bringing it into direct contact with its allosteric activator Rheb via Rag GTPase heterodimers (Zoncu et al., 2011; Inoki et al., 2003; Sancak et al., 2008; Menon et al., 2014). Torin1, which we show causes lysosomal accumulation of AMPK, has also been shown to trigger clustering of inactive mTORC1 on the lysosomal surface (Settembre et al., 2012). If mTORC1 and AMPK do indeed physiologically share identical lysosomal binding partners, then there would either be a requirement for surplus docking sites to compensate for lysosomal clustering of mTORC1 by drug-induced inhibition, or alternatively, α 1- and α 2-subunits take advantage of distinct lysosomal

distinct pools of substrates (i.e., ULK1, autophagosomes; ACC, cytosol, and mitochondria). This is certainly the case for mTORC1, where many of its substrates are cytosolic and phosphorylated long after its dissociation from the lysosomal surface (Manifava et al., 2016). Indeed, it seems likely that mTORC1 phosphorylates cytosolic AMPK, since α 2-S345 phosphorylation in mammalian cells is unaffected by the myristoylation state of the AMPK β -subunit (Ling et al., 2020), a modification that targets AMPK to membrane-bound organelles including lysosomes (Zhang et al., 2017; Liang et al., 2015; Oakhill et al., 2010).

AMPK inhibits mTORC1 directly and indirectly via phosphorylation of raptor and tuberin (also referred to as TSC2), respectively, causing cell-cycle arrest when energy supplies are insufficient for cell division. In addition, aside from its role in autophagy, ULK1 phosphorylates and inhibits leucyl-tRNA synthetase 1 to inhibit mTORC1 in an AMPK-dependent manner (Yoon et al., 2020). We previously demonstrated that amino acid deprivation attenuates cell proliferation, whereas introducing 2-DG (to halt glycolysis) paradoxically enhanced cell proliferation rates, presumably due to the induction of autophagy (Ling et al., 2020), which 2-DG is known to provoke (Xi et al., 2013; Ramirez-Peinado et al., 2013). This supposition was based on the observation that SBI-0206965, a dual AMPK/ULK1 inhibitory compound that blunts autophagy initiation (Egan et al., 2015; Dite et al., 2018), prevented the 2-DG-induced increase in cell proliferation (Ling et al., 2020). As a nutrient recycling system, compensatory mobilization of autophagic flux is frequently observed in highly proliferative cancer cells challenged by the energy-poor tumor microenvironment (Mathew et al., 2007), whereby resultant liberation of amino acids would be sufficient

to reactivate mTORC1. Here, similar to our previous observation using overexpressed AMPK in HEK293 cells (Ling et al., 2020), genetically induced dephosphorylation of α 2-pS345 on endogenous AMPK slowed MEF cell proliferation in amino acid (leucine, arginine, and combined leucine, arginine)-deprived media. AMPK and ULK1 physically dissociate and reassociate with removal and replenishment of nutrients, respectively (Shang et al., 2011), yet proper coordination of ULK1 activity requires initial levels, in nutrient-replete conditions, of concomitant AMPK and mTORC1 phosphorylation on distinct sites including, but not limited to, S555 (AMPK) (Egan et al., 2011) and S757 (mTORC1) (Nwadike et al., 2018). This would explain why we and others (Gordeev et al., 2015) see loss of AMPK-mediated ULK1 phosphorylation upon pharmacological mTORC1 inhibition (i.e., due to AMPK/ULK1 dissociation), and why AMPK and mTORC1 are rapidly and concurrently activated by amino acids following a period of starvation (Dalle Pezze et al., 2016). In the latter instance, CaMKK2 and not LKB1, is the AMPK-activating kinase (Dalle Pezze et al., 2016) that has also been shown to drive autophagy initiation elicited by 2-DG (Xi et al., 2013) as well as various other Ca^{2+} mobilizing agents (Hoyer-Hansen et al., 2007). Altogether, this points to antagonistic functions of α 2-AMPK with mTORC1 to mitigate cellular growth rates in the face of nutrient stress. Unlike LKB1, a *bona fide* tumor suppressor, and its substrate α 2, an emerging tumor suppressor (Vara-Ciruelos et al., 2019), the opposite, tumor-promoting case certainly holds true for CaMKK2 (O'byrne et al., 2020; Asquith et al., 2018) and is similarly emerging for α 1 (Vara-Ciruelos et al., 2019).

Our work conceptually reinforces the lysosome as one of the major intracellular “hubs” that amalgamates AMPK and mTORC1 signal transduction. mTORC1 restrains AMPK activity by direct phosphorylation and sequestration in the cytosol to maximize cellular growth potential conferred by nutrient supply, whereas mTORC1 inhibition and liberation of AMPK imposes a cell growth defect when specific subsets of nutrients (i.e., glucose, amino acids) are limited. That α 2-containing AMPK complexes are subjected to a higher degree of regulatory pressure imposed by mTORC1 in comparison to α 1-complexes, at least in the cell types used in this study, is in agreement with the emerging viewpoint that in certain cancers, α 2 and α 1 function as tumor suppressors and promoters, respectively (Vara-Ciruelos et al., 2019). Inhibition of α 2 would permit cell proliferation to advance with minimal constraints, whereas concomitant α 1 activity and mitigation of processes like autophagy would ensure that cell survival and cellular anabolism are mutually satisfied. The identity of binding partner(s) responsible for trafficking or tethering AMPK complexes specifically containing α 2 to the lysosome following mTORC1 inhibition is a question for further study.

Limitations of the study

Conclusions drawn from our biochemical (Figures 1B–1F, 3A, 3C, and S1), imaging (Figures 4, 5, and S2–S4), and localization (Figure 3C) analyses in mammalian cells should be made with caution given nonspecific effects associated with use of transient expression of AMPK constructs carrying fusion tags. In our experience, expression of AMPK in cultured cells by lipid

transfection or lentiviral transduction methods results in total AMPK protein expression at levels similar to endogenous, suggesting cells are able to tightly control AMPK turnover (Dite et al., 2017). The nature of the fusion tag has been shown to influence allosteric regulation of immunoprecipitated AMPK by palmitoyl-CoA (Pinkosky et al., 2020); however, this was associated more with the method of immobilization, rather than a disruptive effect of affinity tags on AMPK molecular function or conformation. For cell imaging, GFP tags were placed at the N-termini of AMPK α constructs in order to retain myristoylation of β -subunits at position Gly2, a modification important for cellular compartmentalization.

Data are also limited to cell types used; HEK293T cells are amenable to transfection of AMPK complexes, α dKO MEFs were used to allow full control over the expressed α -isoform/mutant, and LKB1-deficient HeLa cells were chosen as these cells display high basal α 2-pS345, which we speculate may arise from impaired AMPK negative feedback on mTORC1 activity. We have no evidence that loss of LKB1-mediated α T172 phosphorylation impairs AMPK lysosomal localization. Consequently, regulatory mechanisms associated with dephosphorylation of α 1-S347 and α 2-S345, in particular those associated with mTORC1/ α 1-AMPK feedback, may differ in more disease-relevant cell models.

STAR★METHODS

Detailed methods are provided in the online version of this paper and include the following:

- KEY RESOURCES TABLE
- RESOURCE AVAILABILITY
 - Lead contact
 - Materials availability
 - Data and code availability
- EXPERIMENTAL MODEL AND SUBJECT DETAILS
 - Mice and ethics statement
 - Immortalised α dKO MEFs
 - Mammalian cell lines
 - Yeast cell lines
- METHOD DETAILS
 - Protein expression constructs
 - Yeast protein preparation
 - Mass spectrometric detection of phospho-peptides
 - Protein expression and purification from *Escherichia coli*
 - Protein expression for mammalian cell-based assays
 - Axin co-immunoprecipitation
 - Immunoblotting
 - AMPK activity assays
 - Phosphorylation assays
 - Lysosome immunoprecipitation
 - Immunofluorescence and image analysis
 - Live cell imaging
 - Fluorescence recovery after photobleaching (FRAP) of mammalian cells
 - Cell proliferation analysis
- QUANTIFICATION AND STATISTICAL ANALYSIS

SUPPLEMENTAL INFORMATION

Supplemental information can be found online at <https://doi.org/10.1016/j.celrep.2022.110365>.

ACKNOWLEDGMENTS

The generation of AMPK α 2-S345A knockin mouse used in this study was supported by Phenomics Australia and the Australian Government through the National Collaborative Research Infrastructure Strategy (NCRIS) program. We thank Benoit Viollet (Institute Cochin) for AMPK α dKO iMEFs and Caroline Palmer (University of Melbourne) for Timm29 and PDI antibodies. S.G., B.E.K., J.W.S., and J.S.O. were supported by National Health and Medical Research Council (NHMRC) project grants (GNT1145836, GNT1138102, and GNT1161262). K.R.M. and J.P. were supported by the NMHRC (GNT1161262), Australian Research Council (DP180101682), a Flinders Foundation seeding grant and Flinders University (Australia). This project was supported by St Vincent's Institute of Medical Research (Australia) and in part by the Victorian Government's Operational Infrastructure Support Program.

AUTHOR CONTRIBUTIONS

K.R.M., W.J.S., N.X.Y.L., A.H., G.S., K.R.W.N., D.Y., and J.P. performed the experiments. L.M.-S. and S.G. supervised mouse and iMEF generation. J.W.S. and B.E.K. provided conceptual input. J.P. and J.S.O. conceived the study, and W.J.S., J.S.O., and J.P. wrote the initial draft. All authors contributed to the final manuscript.

DECLARATION OF INTERESTS

The authors declare no competing interests.

INCLUSION AND DIVERSITY

One or more of the authors of this paper self-identifies as an underrepresented ethnic minority in science. While citing references scientifically relevant for this work, we also actively worked to promote gender balance in our reference list.

Received: April 30, 2021

Revised: October 28, 2021

Accepted: January 19, 2022

Published: February 15, 2022

REFERENCES

Abu-Remaileh, M., Wyant, G.A., Kim, C., Laqtom, N.N., Abbasi, M., Chan, S.H., Freinkman, E., and Sabatini, D.M. (2017). Lysosomal metabolomics reveals V-ATPase- and mTOR-dependent regulation of amino acid efflux from lysosomes. *Science* 358, 807–813.

Asquith, C.R.M., Godoi, P.H., Counago, R.M., Laitinen, T., Scott, J.W., Langendorf, C.G., Oakhill, J.S., Drewry, D.H., Zuercher, W.J., Koutentis, P.A., et al. (2018). 1,2,6-thiadiazinones as novel narrow spectrum calcium/calmodulin-dependent protein kinase kinase 2 (CaMKK2) inhibitors. *Molecules* 23, 1221.

Bain, J., Plater, L., Elliott, M., Shpiro, N., Hastie, C.J., Mclauchlan, H., Klevornic, I., Arthur, J.S., Alessi, D.R., and Cohen, P. (2007). The selectivity of protein kinase inhibitors: a further update. *Biochem. J.* 408, 297–315.

Bimbo, A., Jia, Y., Poh, S.L., Karuturi, R.K., Den Elzen, N., Peng, X., Zheng, L., O'connell, M., Liu, E.T., Balasubramanian, M.K., and Liu, J. (2005). Systematic deletion analysis of fission yeast protein kinases. *Eukaryot. Cell* 4, 799–813.

Caspari, T., Dahlen, M., Kanter-Smoler, G., Lindsay, H.D., Hofmann, K., Papadimitriou, K., Sunnerhagen, P., and Carr, A.M. (2000). Characterization of Schizosaccharomyces pombe Hus1: a PCNA-related protein that associates with Rad1 and Rad9. *Mol. Cell. Biol.* 20, 1254–1262.

Coughlan, K.A., Valentine, R.J., Sudit, B.S., Allen, K., Dagon, Y., Kahn, B.B., Ruderman, N.B., and Saha, A.K. (2016). PKD1 inhibits AMPK α 2 through

phosphorylation of serine 491 and impairs insulin signaling in skeletal muscle cells. *J. Biol. Chem.* 291, 5664–5675.

Dagon, Y., Hur, E., Zheng, B., Wellenstein, K., Cantley, L.C., and Kahn, B.B. (2012). p70S6 kinase phosphorylates AMPK on serine 491 to mediate leptin's effect on food intake. *Cell Metab.* 16, 104–112.

Dalle Pezze, P., Ruf, S., Sonntag, A.G., Langelaar-Makkinje, M., Hall, P., Heberle, A.M., Razquin Navas, P., Van Eunen, K., Tolle, R.C., Schwarz, J.J., et al. (2016). A systems study reveals concurrent activation of AMPK and mTOR by amino acids. *Nat. Commun.* 7, 13254.

Dite, T.A., Langendorf, C.G., Hoque, A., Galic, S., Rebello, R.J., Ovens, A.J., Lindqvist, L.M., Ngoei, K.R.W., Ling, N.X.Y., Furic, L., et al. (2018). AMP-activated protein kinase selectively inhibited by the type II inhibitor SBI-0206965. *J. Biol. Chem.* 293, 8874–8885.

Dite, T.A., Ling, N.X.Y., Scott, J.W., Hoque, A., Galic, S., Parker, B.L., Ngoei, K.R.W., Langendorf, C.G., O'brien, M.T., Kundu, M., et al. (2017). The autophagy initiator ULK1 sensitizes AMPK to allosteric drugs. *Nat. Commun.* 8, 571.

Egan, D.F., Chun, M.G., Vamos, M., Zou, H., Rong, J., Miller, C.J., Lou, H.J., Raveendra-Panickar, D., Yang, C.C., Sheffler, D.J., et al. (2015). Small molecule inhibition of the autophagy kinase ULK1 and identification of ULK1 substrates. *Mol. Cell* 59, 285–297.

Egan, D.F., Shackelford, D.B., Mihaylova, M.M., Gelino, S., Kohnz, R.A., Mair, W., Vasquez, D.S., Joshi, A., Gwinn, D.M., Taylor, R., et al. (2011). Phosphorylation of ULK1 (hATG1) by AMP-activated protein kinase connects energy sensing to mitophagy. *Science* 331, 456–461.

Garcia, D., and Shaw, R.J. (2017). AMPK: mechanisms of cellular energy sensing and restoration of metabolic balance. *Mol. Cell* 66, 789–800.

Gordeev, S.A., Bykova, T.V., Zubova, S.G., Bystrova, O.A., Martynova, M.G., Pospelov, V.A., and Pospelova, T.V. (2015). mTOR kinase inhibitor pp242 causes mitophagy terminated by apoptotic cell death in E1A-Ras transformed cells. *Oncotarget* 6, 44905–44926.

Gwinn, D.M., Shackelford, D.B., Egan, D.F., Mihaylova, M.M., Mery, A., Vasquez, D.S., Turk, B.E., and Shaw, R.J. (2008). AMPK phosphorylation of raptor mediates a metabolic checkpoint. *Mol. Cell* 30, 214–226.

Hawley, S.A., Ross, F.A., Gowans, G.J., Tibarewal, P., Leslie, N.R., and Hardie, D.G. (2014). Phosphorylation by Akt within the ST loop of AMPK- α 1 down-regulates its activation in tumour cells. *Biochem. J.* 459, 275–287.

Heathcote, H.R., Mancini, S.J., Strembitska, A., Jamal, K., Reihill, J.A., Palmer, T.M., Gould, G.W., and Salt, I.P. (2016). Protein kinase C phosphorylates AMP-activated protein kinase α 1 Ser487. *Biochem. J.* 473, 4681–4697.

Horman, S., Vertommen, D., Heath, R., Neumann, D., Mouton, V., Woods, A., Schlattner, U., Wallimann, T., Carling, D., Hue, L., and Rider, M.H. (2006). Insulin antagonizes ischemia-induced Thr172 phosphorylation of AMP-activated protein kinase α -subunits in heart via hierarchical phosphorylation of Ser485/491. *J. Biol. Chem.* 281, 5335–5340.

Hornbeck, P.V., Zhang, B., Murray, B., Kornhauser, J.M., Latham, V., and Skrzypek, E. (2015). PhosphoSitePlus, 2014: mutations, PTMs and recalibrations. *Nucleic Acids Res.* 43, D512–D520.

Hoyer-Hansen, M., Bastholm, L., Szyniarowski, P., Campanella, M., Szabadkai, G., Farkas, T., Bianchi, K., Fehrenbacher, N., Elling, F., Rizzuto, R., et al. (2007). Control of macroautophagy by calcium, calmodulin-dependent kinase kinase- β , and Bcl-2. *Mol. Cell* 25, 193–205.

Hurley, R.L., Barre, L.K., Wood, S.D., Anderson, K.A., Kemp, B.E., Means, A.R., and Witters, L.A. (2006). Regulation of AMP-activated protein kinase by multisite phosphorylation in response to agents that elevate cellular cAMP. *J. Biol. Chem.* 281, 36662–36672.

Inoki, K., Li, Y., Xu, T., and Guan, K.L. (2003). Rheb GTPase is a direct target of TSC2 GAP activity and regulates mTOR signaling. *Genes Dev.* 17, 1829–1834.

Iseli, T.J., Oakhill, J.S., Bailey, M.F., Wee, S., Walter, M., Van Denderen, B.J., Castelli, L.A., Katsis, F., Witters, L.A., Stapleton, D., et al. (2008). AMP-activated protein kinase subunit interactions: beta1:gamma1 association requires beta1 Thr-263 and Tyr-267. *J. Biol. Chem.* 283, 4799–4807.

- Kang, S.A., Pacold, M.E., Cervantes, C.L., Lim, D., Lou, H.J., Ottina, K., Gray, N.S., Turk, B.E., Yaffe, M.B., and Sabatini, D.M. (2013). mTORC1 phosphorylation sites encode their sensitivity to starvation and rapamycin. *Science* **341**, 1236566.
- Laplanche, M., and Sabatini, D.M. (2012). mTOR signaling in growth control and disease. *Cell* **149**, 274–293.
- Lawrence, R.E., Cho, K.F., Rappold, R., Thrun, A., Tofaute, M., Kim, D.J., Moldavski, O., Hurley, J.H., and Zoncu, R. (2018). A nutrient-induced affinity switch controls mTORC1 activation by its Rag GTPase-regulator lysosomal scaffold. *Nat. Cell Biol.* **20**, 1052–1063.
- Liang, J., Xu, Z.X., Ding, Z., Lu, Y., Yu, Q., Werle, K.D., Zhou, G., Park, Y.Y., Peng, G., Gambello, M.J., and Mills, G.B. (2015). Myristoylation confers non-canonical AMPK functions in autophagy selectivity and mitochondrial surveillance. *Nat. Commun.* **6**, 7926.
- Ling, N.X.Y., Kaczmarek, A., Hoque, A., Davie, E., Ngoei, K.R.W., Morrison, K.R., Smiles, W.J., Forte, G.M., Wang, T., Lie, S., et al. (2020). mTORC1 directly inhibits AMPK to promote cell proliferation under nutrient stress. *Nat. Metab.* **2**, 41–49.
- Liu, Q., Kirubakaran, S., Hur, W., Niepel, M., Westover, K., Thoreen, C.C., Wang, J., Ni, J., Patricelli, M.P., Vogel, K., et al. (2012). Kinome-wide selectivity profiling of ATP-competitive mammalian target of rapamycin (mTOR) inhibitors and characterization of their binding kinetics. *J. Biol. Chem.* **287**, 9742–9752.
- Manders, E.M., Stap, J., Brakenhoff, G.J., Van Driel, R., and Aten, J.A. (1992). Dynamics of three-dimensional replication patterns during the S-phase, analysed by double labelling of DNA and confocal microscopy. *J. Cell Sci.* **103**, 857–862.
- Manders, E.M.M., Verbeek, F.J., and Aten, J.A. (1993). Measurement of co-localization of objects in dual-colour confocal images. *J. Microsc. Oxford* **169**, 375–382.
- Manifava, M., Smith, M., Rotondu, S., Walker, S., Niewczas, I., Zoncu, R., Clark, J., and Kistakis, N.T. (2016). Dynamics of mTORC1 activation in response to amino acids. *Elife* **5**, e19960.
- Mathew, R., Karantza-Wadsworth, V., and White, E. (2007). Role of autophagy in cancer. *Nat. Rev. Cancer* **7**, 961–967.
- Menon, S., Dibble, C.C., Talbott, G., Hoxhaj, G., Valvezan, A.J., Takahashi, H., Cantley, L.C., and Manning, B.D. (2014). Spatial control of the TSC complex integrates insulin and nutrient regulation of mTORC1 at the lysosome. *Cell* **156**, 771–785.
- Ngoei, K.R.W., Langendorf, C.G., Ling, N.X.Y., Hoque, A., Varghese, S., Camerino, M.A., Walker, S.R., Bozikis, Y.E., Dite, T.A., Ovens, A.J., et al. (2018). Structural determinants for small-molecule activation of skeletal muscle AMPK $\alpha 2\beta 2\gamma 1$ by the glucose importagoc SC4. *Cell Chem. Biol.* **25**, 728–737 e729.
- Nwadike, C., Williamson, L.E., Gallagher, L.E., Guan, J.L., and Chan, E.Y.W. (2018). AMPK inhibits ULK1-dependent autophagosome formation and lysosomal acidification via distinct mechanisms. *Mol. Cell. Biol.* **38**, e00023-18.
- O'byrne, S.N., Scott, J.W., Pilote, J.R., Santiago, A.D.S., Langendorf, C.G., Oakhill, J.S., Eduful, B.J., Counago, R.M., Wells, C.I., Zuercher, W.J., et al. (2020). In depth analysis of kinase cross screening data to identify CAMKK2 inhibitory scaffolds. *Molecules* **25**, 325.
- Oakhill, J.S., Chen, Z.P., Scott, J.W., Steel, R., Castelli, L.A., Ling, N., Macaulay, S.L., and Kemp, B.E. (2010). β -Subunit myristoylation is the gatekeeper for initiating metabolic stress sensing by AMP-activated protein kinase (AMPK). *Proc. Natl. Acad. Sci. U.S.A.* **107**, 19237–19241.
- Oakhill, J.S., Scott, J.W., and Kemp, B.E. (2012). AMPK functions as an adenylate charge-regulated protein kinase. *Trends Endocrinol. Metab.* **23**, 125–132.
- Orozco, J.M., Krawczyk, P.A., Scaria, S.M., Cangelosi, A.L., Chan, S.H., Kunchok, T., Lewis, C.A., and Sabatini, D.M. (2020). Dihydroxyacetone phosphate signals glucose availability to mTORC1. *Nat. Metab.* **2**, 893–901.
- Pinkosky, S.L., Scott, J.W., Desjardins, E.M., Smith, B.K., Day, E.A., Ford, R.J., Langendorf, C.G., Ling, N.X.Y., Nero, T.L., Loh, K., et al. (2020). Long-chain fatty acyl-CoA esters regulate metabolism via allosteric control of AMPK $\beta 1$ isoforms. *Nat. Metab.* **2**, 873–881.
- Puustinen, P., Keldsbo, A., Corcelle-Termeau, E., Ngoei, K., Sonder, S.L., Farakas, T., Kaae Andersen, K., Oakhill, J.S., and Jaattela, M. (2020). DNA-dependent protein kinase regulates lysosomal AMP-dependent protein kinase activation and autophagy. *Autophagy* **16**, 1–18.
- Ramirez-Peinado, S., Leon-Annicchiarico, C.L., Galindo-Moreno, J., Iurlaro, R., Caro-Maldonado, A., Prehn, J.H., Ryan, K.M., and Munoz-Pinedo, C. (2013). Glucose-starved cells do not engage in prosurvival autophagy. *J. Biol. Chem.* **288**, 30387–30398.
- Sancak, Y., Peterson, T.R., Shaul, Y.D., Lindquist, R.A., Thoreen, C.C., Bar-Peled, L., and Sabatini, D.M. (2008). The Rag GTPases bind raptor and mediate amino acid signaling to mTORC1. *Science* **320**, 1496–1501.
- Scott, J.W., Ling, N., Issa, S.M., Dite, T.A., O'brien, M.T., Chen, Z.P., Galic, S., Langendorf, C.G., Steinberg, G.R., Kemp, B.E., and Oakhill, J.S. (2014). Small molecule drug A-769662 and AMP synergistically activate naive AMPK independent of upstream kinase signaling. *Chem. Biol.* **27**, 619–627.
- Scott, J.W., Van Denderen, B.J., Jorgensen, S.B., Honeyman, J.E., Steinberg, G.R., Oakhill, J.S., Iseli, T.J., Koay, A., Gooley, P.R., Stapleton, D., and Kemp, B.E. (2008). Thienopyridone drugs are selective activators of AMP-activated protein kinase $\beta 1$ -containing complexes. *Chem. Biol.* **15**, 1220–1230.
- Settembre, C., Zoncu, R., Medina, D.L., Vetrini, F., Erdin, S., Erdin, S., Huynh, T., Ferron, M., Karsenty, G., Vellard, M.C., et al. (2012). A lysosome-to-nucleus signalling mechanism senses and regulates the lysosome via mTOR and TFEB. *EMBO J.* **31**, 1095–1108.
- Shang, L., Chen, S., Du, F., Li, S., Zhao, L., and Wang, X. (2011). Nutrient starvation elicits an acute autophagic response mediated by Ulk1 dephosphorylation and its subsequent dissociation from AMPK. *Proc. Natl. Acad. Sci. U.S.A.* **108**, 4788–4793.
- Shin, S., Wolgamott, L., Tcherkezian, J., Vallabhapurapu, S., Yu, Y., Roux, P.P., and Yoon, S.O. (2014). Glycogen synthase kinase-3 β positively regulates protein synthesis and cell proliferation through the regulation of translation initiation factor 4E-binding protein 1. *Oncogene* **33**, 1690–1699.
- Shin, S., Wolgamott, L., Yu, Y., Blenis, J., and Yoon, S.O. (2011). Glycogen synthase kinase (GSK)-3 promotes p70 ribosomal protein S6 kinase (p70S6K) activity and cell proliferation. *Proc. Natl. Acad. Sci. U.S.A.* **108**, E1204–E1213.
- Steen, H., Jebanathirajah, J.A., Springer, M., and Kirschner, M.W. (2005). Stable isotope-free relative and absolute quantitation of protein phosphorylation stoichiometry by MS. *Proc. Natl. Acad. Sci. U.S.A.* **102**, 3948–3953.
- Suzuki, T., Bridges, D., Nakada, D., Skiniotis, G., Morrison, S.J., Lin, J.D., Saltiel, A.R., and Inoki, K. (2013). Inhibition of AMPK catabolic action by GSK3. *Mol. Cell* **50**, 407–419.
- Thoreen, C.C., Kang, S.A., Chang, J.W., Liu, Q., Zhang, J., Gao, Y., Reichling, L.J., Sim, T., Sabatini, D.M., and Gray, N.S. (2009). An ATP-competitive mammalian target of rapamycin inhibitor reveals rapamycin-resistant functions of mTORC1. *J. Biol. Chem.* **284**, 8023–8032.
- Vara-Ciruelos, D., Russell, F.M., and Hardie, D.G. (2019). The strange case of AMPK and cancer: Dr Jekyll or Mr Hyde? (dagger). *Open Biol.* **9**, 190099.
- Warden, S.M., Richardson, C., O'donnell, J., Jr., Stapleton, D., Kemp, B.E., and Witters, L.A. (2001). Post-translational modifications of the β -1 subunit of AMP-activated protein kinase affect enzyme activity and cellular localization. *Biochem. J.* **354**, 275–283.
- Xi, H., Barredo, J.C., Merchan, J.R., and Lampidis, T.J. (2013). Endoplasmic reticulum stress induced by 2-deoxyglucose but not glucose starvation activates AMPK through CaMKK β leading to autophagy. *Biochem. Pharmacol.* **85**, 1463–1477.
- Yoon, I., Nam, M., Kim, H.K., Moon, H.S., Kim, S., Jang, J., Song, J.A., Jeong, S.J., Kim, S.B., Cho, S., et al. (2020). Glucose-dependent control of leucine metabolism by leucyl-tRNA synthetase 1. *Science* **367**, 205–210.

Zhang, C.S., Hawley, S.A., Zong, Y., Li, M., Wang, Z., Gray, A., Ma, T., Cui, J., Feng, J.W., Zhu, M., et al. (2017). Fructose-1,6-bisphosphate and aldolase mediate glucose sensing by AMPK. *Nature* 548, 112–116.

Zhang, C.S., Jiang, B., Li, M., Zhu, M., Peng, Y., Zhang, Y.L., Wu, Y.Q., Li, T.Y., Liang, Y., Lu, Z., et al. (2014). The lysosomal v-ATPase-Ragulator complex is a common activator for AMPK and mTORC1, acting as a switch between catabolism and anabolism. *Cell Metab.* 20, 526–540.

Zhang, C.S., Li, M., Zong, Y., and Lin, S.C. (2018). Determining AMPK activation via the lysosomal v-ATPase-ragulator-AXIN/LKB1 Axis. *Methods Mol. Biol.* 1732, 393–411.

Zoncu, R., Bar-Peled, L., Efeyan, A., Wang, S., Sancak, Y., and Sabatini, D.M. (2011). mTORC1 senses lysosomal amino acids through an inside-out mechanism that requires the vacuolar H(+)-ATPase. *Science* 334, 678–683.

STAR★METHODS

KEY RESOURCES TABLE

| REAGENT or RESOURCE | SOURCE | IDENTIFIER |
|--|---|---|
| Antibodies | | |
| pan AMPK α (monoclonal mouse) | Cell Signaling Technology | Cat# 2793; RRID: AB_915794 |
| ULK1 (polyclonal rabbit) | Cell Signaling Technology | Cat# 4773; clone R600; RRID: AB_2288252 |
| p70 S6K (monoclonal rabbit) | Cell Signaling Technology | Cat# 9202; RRID: AB_331676 |
| 4E-BP1 (monoclonal rabbit) | Cell Signaling Technology | Cat# 9452; RRID: AB_331692 |
| α -Tubulin (monoclonal mouse) | Cell Signaling Technology | Cat# 3873; clone DM1A; RRID: AB_1904178 |
| Axin1 (monoclonal rabbit) | Cell Signaling Technology | Cat# 2087; clone C76H11; RRID: AB_2274550 |
| Lamin A/C (monoclonal mouse) | Cell Signaling Technology | Cat# 4777; clone 4C11; RRID: AB_10545756 |
| LAMP1 (monoclonal rabbit) | Cell Signaling Technology | Cat# 9091; clone D2D11; RRID: AB_2687579 |
| GAPDH (monoclonal rabbit) | Cell Signaling Technology | Cat# 5174; clone D16H11; RRID: AB_10622025 |
| Rab11a (polyclonal rabbit) | Cell Signaling Technology | Cat# 2413; RRID: AB_2173452 |
| Syntaxin 6 (monoclonal rabbit) | Cell Signaling Technology | Cat# 2869; clone C34B2; RRID: AB_2196500 |
| TIMM29 (polyclonal rabbit) | Sigma-Aldrich | Cat# HPA041858; RRID: AB_10963429 |
| PEX14 (polyclonal rabbit) | Proteintech | Cat# 10594-1-AP; RRID: AB_2252194 |
| PDI (monoclonal mouse) | Enzo Life Sciences | Cat# ADI-SPA-891; clone ID3; RRID: AB_10615355 |
| AMPK α pT172 (monoclonal rabbit) | Cell Signaling Technology | Cat# 2535; RRID: AB_331250 |
| AMPK α 1 pS347 | Eurogentech SA; Ling et al., 2020 | N/A |
| AMPK α 1 pT479 | Merck Millipore | Cat# ABS981 |
| AMPK α 2 pS345 (monoclonal rabbit) | Abcam | Cat# ab129081; clone EMPDAR6; RRID: AB_11155357 |
| ACC pS79/S212 (polyclonal rabbit) | Cell Signaling Technology | Cat# 3661; RRID: AB_330337 |
| ULK1 pS555 (monoclonal rabbit) | Cell Signaling Technology | Cat# 5869; clone D1H4; RRID: AB_10707365 |
| ULK1 pS757 (polyclonal rabbit) | Cell Signaling Technology | Cat# 6888; RRID: AB_10829226 |
| p70 S6K pT389 (polyclonal rabbit) | Cell Signaling Technology | Cat# 9205; RRID: AB_330944 |
| 4E-BP1 pT37/T46 (polyclonal rabbit) | Cell Signaling Technology | Cat# 9459; RRID: AB_330985 |
| Glycogen synthase pS641 (polyclonal rabbit) | Cell Signaling Technology | Cat# 3891; RRID: AB_2116390 |
| IRDye 680RD (goat anti-rabbit IgG) | LI-COR Biosciences | Cat# LCR-926-68071; RRID: AB_10956166 |
| IRDye 800CW (goat anti-rabbit IgG) | LI-COR Biosciences | Cat# LCR-926-32210; RRID: AB_621842 |
| Alexa Fluor 647 (goat anti-rabbit IgG) | Thermo Fisher Scientific | Cat# A-21245; RRID: AB_2535813 |
| Chemicals, Peptides, and Recombinant Proteins | | |
| Torin-1 | Selleck Chemicals | Cat# S2827 |
| Rapamycin | Sigma-Aldrich | Cat# R8781 |
| CHIR99021 | Sigma-Aldrich | Cat# SML1046 |
| 2-deoxy-D-glucose | Sigma-Aldrich | Cat# D8375 |
| Fluoroshield™ with DAPI | Sigma-Aldrich | Cat# F6057 |
| FM4-64 | Biotium | Cat# 70021 |
| FuGENE HD | Promega | Cat# E2311 |
| Lipofectamine 2000 | Invitrogen | Cat# 1168-027 |
| GSK3 β | Sigma-Aldrich | Cat# 14-306 |
| mTORC1 | Sigma-Aldrich | Cat# SRP0364 |
| cOmplete protease inhibitor cocktail | Sigma-Aldrich | Cat# 11697498001 |
| L-arginine | Sigma-Aldrich | Cat# A6969 |
| L-glutamine | Sigma-Aldrich | Cat# G7513 |
| L-leucine | Sigma-Aldrich | Cat# W329703 |

(Continued on next page)

| REAGENT or RESOURCE | SOURCE | IDENTIFIER |
|---|-------------------------------------|------------------------|
| L-lysine | Sigma-Aldrich | Cat# L5626 |
| Penicillin-streptomycin | Sigma-Aldrich | Cat# P0781 |
| Sodium bicarbonate | Sigma-Aldrich | Cat# S5761 |
| SAMS synthetic peptide substrate HMRSAMSGHLHLVKRR-NH2 | Purar Chemicals | N/A |
| [γ - ³² P] ATP | PerkinElmer | Cat# BLU002Z500UC |
| Experimental models: Cell lines | | |
| <i>S. pombe</i> wild type: <i>h⁻ leu1.32</i> | Bimbo et al. (2005) | Laboratory ref.: JP305 |
| <i>S. pombe</i> <i>gsk3Δ: h⁻ gsk3::ura4+ leu1.32</i> | Bimbo et al. (2005) | Laboratory ref.: JP534 |
| HeLa | American Type Culture Collection | Cat# CCL-2 |
| HEK293 | American Type Culture Collection | Cat# CRL-157 |
| HEK293T | American Type Culture Collection | Cat# CRL3216 |
| AMPK $\alpha 1^{-/-}/\alpha 2^{-/-}$ (α dKO) immortalized mouse embryonic fibroblasts | Dite et al. (2017) | N/A |
| AMPK $\alpha 2^{S345A}$ immortalized mouse embryonic fibroblasts | This study | N/A |
| Experimental models: Organisms/Strains | | |
| Mouse: C57/BL/6J AMPK $\alpha 2^{S345A}$ | This study | N/A |
| Oligonucleotides | | |
| Human AMPK $\alpha 1$ S347A For: CTATTTGGCGACAGCCCCACCTGATTCTTTTC | Sigma-Aldrich | Laboratory ref.: A188 |
| Human AMPK $\alpha 1$ S347A Rev: GAAAAGAATCAGGTGGGGCTGTGCGCAAATAG | Sigma-Aldrich | Laboratory ref.: A189 |
| Human AMPK $\alpha 1$ S347E For: CTATTTGGCGACAGAACCACCTGATTCTTTTC | Sigma-Aldrich | Laboratory ref.: A192 |
| Human AMPK $\alpha 1$ S347E Rev: GAAAAGAATCAGGTGGTTCTGTGCGCAAATAG | Sigma-Aldrich | Laboratory ref.: A193 |
| Human AMPK $\alpha 2$ S345A For: CCTCGCCTCTGCTCCTCCATCTGG | Ling et al. (2020) | Laboratory ref.: A176 |
| Human AMPK $\alpha 2$ S345A Rev: CCAGATGGAGGAGCAGAGGCGAGG | Ling et al. (2020) | Laboratory ref.: A177 |
| Human AMPK $\alpha 2$ S345E For: CCTCGCCTCTGAACCTCCATCTGG | Ling et al. (2020) | Laboratory ref.: A180 |
| Human AMPK $\alpha 2$ S345E Rev: CCAGATGGAGGTTCCAGAGGCGAGG | Ling et al. (2020) | Laboratory ref.: A181 |
| Rat AMPK $\alpha 2$ S345A For: CCTCGCCTCCGCTCCTCCAACGG | This study | Laboratory ref.: A238 |
| Rat AMPK $\alpha 2$ S345A Rev: CCGTTGGAGGAGCGGAGGCGAGG | This study | Laboratory ref.: A239 |
| Rat AMPK $\alpha 2$ S345E For: CCTCGCCTCCGAACCTCCAACGG | This study | Laboratory ref.: A240 |
| Rat AMPK $\alpha 2$ S345E Rev: CCGTTGGAGGTTCCGAGGCGAGG | This study | Laboratory ref.: A241 |
| sgRNA: AGAACCTGATGGAGGACTAG | This study | N/A |
| Oligo donor $\alpha 2$ S345A: CTTATCATCTTATCATTGACAATCGGAG AATAATGAACCAAGCCAGTGAGTTCTA CCTCGCATCTGCCCTCCATCAGGTTT TTTTATGGATGACAGCGCCATGCATATT CCTCCAGGCTTGAACCA | This study | N/A |

(Continued on next page)

Continued

| REAGENT or RESOURCE | SOURCE | IDENTIFIER |
|--|--|---|
| Recombinant DNA | | |
| pET DUET human AMPK α 1 D141A (N-term 6xhis fusion)/ γ 1 | Ngoei et al. (2018) | Laboratory ref.: P710 |
| pET DUET human AMPK α 2 D139A (N-term 6xhis fusion)/ γ 1 | Ngoei et al. (2018) | Laboratory ref.: P893 |
| pET RSF DUET human AMPK β 1/NMT | Oakhill et al. (2010) | Laboratory ref.: P555 |
| pEGFP.C1 human AMPK α 1 (N-term EGFP fusion) | This study | Laboratory ref.: P1361 |
| pEGFP.C1 human AMPK α 1 S347A (N-term EGFP fusion) | This study | Laboratory ref.: P1362 |
| pEGFP.C1 human AMPK α 1 S347E (N-term EGFP fusion) | This study | Laboratory ref.: P1361 |
| pEGFP.C1 rat AMPK α 2 (N-term EGFP fusion) | This study | Laboratory ref.: P306 |
| pEGFP.C1 rat AMPK α 2 S345A (N-term EGFP fusion) | This study | Laboratory ref.: P1286 |
| pEGFP.C1 rat AMPK α 2 S345E (N-term EGFP fusion) | This study | Laboratory ref.: P1337 |
| pDEST27 human AMPK α 1 (N-term GST fusion) | Scott et al. (2014) | Laboratory ref.: P73 |
| pcDNA3 human AMPK β 1 (C-term FLAG fusion) | Scott et al. (2014) | Laboratory ref.: P578 |
| pcDNA3 human AMPK β 1 (C-term myc fusion) | Scott et al. (2014) | Laboratory ref.: P512 |
| pMT2 human AMPK γ 1 (N-term HA fusion) | Iseli et al. (2008) | Laboratory ref.: P135 |
| pBSSVD2005 SV40 large-T antigen expression | Gift, D Ron | Addgene RRID: 21826 |
| pLJC5-TMEM192 (C-term 3xHA fusion) | Gift, D. Sabatini; Abu-Remaileh et al., 2017 | Addgene RRID: 102930 |
| psPax2 | Gift, D. Trono | Addgene RRID: 12260 |
| pHCMV-EcoEnv | Gift, M Sena-Esteves | Addgene RRID: 15802 |
| LeGO-iG2 human AMPK α 1 (C-term FLAG fusion) | Ngoei et al. (2018) | Laboratory ref.: P977 |
| LeGO-iG2 human AMPK α 1 S347A (C-term FLAG fusion) | This study | Laboratory ref.: P1415 |
| LeGO-iG2 human AMPK α 1 S347E (C-term FLAG fusion) | This study | Laboratory ref.: P1416 |
| LeGO-iG2 human AMPK α 2 (C-term FLAG fusion) | Ngoei et al. (2018) | Laboratory ref.: P1135 |
| LeGO-iG2 human AMPK α 2 S345A (C-term FLAG fusion) | Ngoei et al. (2018) | Laboratory ref.: P1168 |
| LeGO-iG2 human AMPK α 2 S345E (C-term FLAG fusion) | Ngoei et al. (2018) | Laboratory ref.: P1170 |
| Other | | |
| IRDye 680RD labelled Streptavidin | LI-COR Biosciences | Cat# 926-68079 |
| Glutathione Sepharose 4B | GE Life Sciences | Cat# 17-0756-01 |
| Streptavidin Sepharose high-performance | GE Life Sciences | Cat# 17-5113-01 |
| Anti-FLAG M2 affinity gel | Sigma-Aldrich | Cat# D2220 |
| EZview red anti-HA affinity gel | Sigma-Aldrich | Cat# E6779 |
| QuikChange II site-directed mutagenesis kit | Agilent Technologies | Cat# 200523 |
| Cation-exchange paper | Produced in-house | https://www.svi.edu.au/resources/phosphocellulose_paper/ |
| DMEM, high glucose | Thermo Fisher Scientific | Cat# 11965084 |
| DMEM, high glucose, arginine/lysine/leucine free | Thermo Fisher Scientific | Cat# 88425 |

RESOURCE AVAILABILITY

Lead contact

Further information and requests for resources and reagents should be directed to and will be fulfilled by the lead contact, Jonathan Oakhill (joakhill@svi.edu.au).

Materials availability

Plasmids, cell lines, and mouse lines generated in this study are available upon request.

Data and code availability

- All data reported in this paper will be shared by the lead contacts upon request.
- This paper does not report original code.
- Any additional information required to reanalyze the data reported in this paper is available from the lead contacts upon request.

EXPERIMENTAL MODEL AND SUBJECT DETAILS

Mice and ethics statement

All mouse studies complied with relevant ethical regulations and approved by the Walter and Eliza Hall Institute Animal Ethics Committee. The *AMPK α 2-S345A* mouse was generated by the MAGEC laboratory (WEHI) on a C57BL/6J background. 20 ng μL^{-1} of Cas9 mRNA, 10 ng μL^{-1} of sgRNA and 40 ng μL^{-1} of the oligo donor were injected into the cytoplasm of fertilized one-cell stage embryos generated from wild-type C57BL/6J breeders. Twenty-four hours later, two-cell stage embryos were transferred into the uteri of pseudo-pregnant female mice. Viable offspring were genotyped by next-generation sequencing. Targeted animals were backcrossed twice to wild-type C57BL/6J to eliminate off-target mutations.

Mice were euthanised via cervical dislocation and doused with 70% ethanol. Using fine forceps and scissors, the tibialis anterior; extensor digitorum and liver were dissected and immediately snap frozen in an Eppendorf submerged in liquid nitrogen and then stored at -80°C . Samples stored at -80°C were placed on dry ice next to an inverted petri dish. Using a scalpel blade, a small piece of tissue was cut from each frozen sample and transferred to an Eppendorf tube stored on dry ice. Samples were transferred to a glass tube containing 300 μL cell lysis buffer [50 mM HEPES (pH 7.4), 150 mM NaCl, 50 mM NaF, 5 mM sodium pyrophosphate, 5 mM EDTA, 1 mM DTT, 250 mM sucrose, 1% Triton-X with protease inhibitors] on wet ice. Tissue was homogenised before being transferred to an Eppendorf tube and centrifuged at 14,000 rpm for 5 mins at 4°C . Avoiding the pellet and top layer of foam, the supernatant was transferred to another Eppendorf tube and stored at -80°C before immunoblotting for AMPK α 2-pS345 and total AMPK α .

Immortalised α dKO MEFs

To generate the α 2-S345A immortalised MEF (iMEF) cell line, MEFs were extracted from homozygous AMPK α 2S345A embryos (days 12–14 post-coitum). MEFs were immortalized by Fugene HD-mediated transfection with an SV40 large-T antigen expression construct. α 2-S345A iMEF cells were maintained in high-glucose DMEM supplemented with 10% FBS at 37°C with 5% CO_2 .

Mammalian cell lines

HeLa (CCL-2), HEK293 (CRL-157) and HEK293T (CRL-3216) cells were purchased from the American Type Culture Collection (ATCC). α dKO MEFs were extracted from homozygous AMPK-null α 1 $^{-/-}$ / α 2 $^{-/-}$ embryos (12–14 d post-coitum) and immortalized by FuGENE HD-mediated transfection with an SV40 large T antigen expression construct (Dite et al., 2017). All cell lines were maintained in high-glucose DMEM supplemented with 10% FBS at 37°C with 5% CO_2 .

Yeast cell lines

Wild type *h⁺ leu1.32* (JP305 - lab stock) and *h⁻ gsk3::ura4+ leu1.32* (JP534) were used (Bimbo et al., 2005). Cells were cultured at 28°C in Edinburgh minimal medium (EMM2) with 5 g l^{-1} NH_4Cl (EMM) as a nitrogen source. Cells were grown exponentially for 48 h.

METHOD DETAILS

Protein expression constructs

All constructs and mutants were sequence verified. cDNAs for human AMPK α 1 and α 2 (WT, and S345/7A and S345/7E mutants) were generated with a C-terminal FLAG-tag and cloned into LeGO-iG2 using EcoRI/NotI restriction sites. Ecotropic lentivirus was generated by transient transfection of HEK293T cells using calcium phosphate, as described previously (Dite et al., 2017). cDNAs for rat AMPK α 1 and α 2 (WT, and S345/7A and S345/7E mutants) were cloned into pEGFP.C1 using XhoI/EcoRI restriction sites to generate N-terminal GFP-fusion proteins.

Yeast protein preparation

A trichloroacetic acid precipitation protocol was followed for *S. pombe* total protein extracts (Caspari et al., 2000). Briefly, cells were harvested by filtration and snap frozen in liquid nitrogen. 20% TCA was added to the cell pellet. The precipitate was homogenised in the Ribolyser MP FastPrep-24 with glass beads for 6 sec and transferred to a new Eppendorf tube along with 5% TCA used to wash the beads. The protein was pelleted at 13,000 rpm for 3 min at 4°C and resuspended in protein loading buffer with 10% DTT (10 mM),

the pH was brought back to (pH 8) with 1 M Tris. The following dilutions of antibodies were used in this study: rabbit anti-Ssp2 and rabbit anti-Ssp2-pSer367 (1:500 and 1:2000 raised by Eurogentec SA, Seraing, Belgium), Alkaline phosphatase coupled secondary antibodies were used for all blots followed by direct detection with NBT/BCIP (VWR) substrates on PVDF membranes.

Mass spectrometric detection of phospho-peptides

FLAG-tagged AMPK immobilised on FLAG resin was precipitated by 800 μ L of ice-cold methanol for 30 min. Following centrifugation (12,000 \times *g*, 10 min) and removal of the supernatant, FLAG beads were dried under nitrogen stream and reconstituted in 50 μ L of 50 mM Tris (pH 7.6). 200 ng of sequencing-grade trypsin was added to the samples for digestion and incubated overnight at 37°C with agitation. This reaction was quenched with 1 μ L formic acid and tryptic peptides were analysed using a Dionex Ultimate 3000 UPLC (Dionex, Idstein, Germany) coupled to a TripleTOF 5600 QqTOF mass spectrometer (AB Sciex, Concord, Canada) equipped with a Turbo V™ dual-ion source. 20 μ L of tryptic peptides were injected and separated on a Waters ACQUITY UPLC™ BEH C18 column (100 mm \times 2.1 mm, 1.7 μ m) at a flow rate of 125 μ L/min under a linear gradient based on two mobile phases. Mobile phase A, 0.1% formic acid in water, and mobile phase B, 0.1% formic acid and acetonitrile/water 9:1 (v/v) were applied using the following parameters: 2.5% B for 2.5 min, a linear increase to 60% B for 67.5 min, an increase to 95% B for 5 min and holding for 10 min, then re-equilibrated to the starting conditions for 5 min. Data were acquired on TOF-MS1 scan to obtain MS1 intensity for the calculation of phosphorylation stoichiometries and product ion scan to obtain MS/MS spectra for peptide sequence confirmation. ESI parameters were optimized and preset for all measurements as follows: Source temperature, 300°C; Curtain gas, 15 psi; Gas 1, 35 psi; Gas 2, 35 psi; declustering potential (DP): +100 V; Ion spray voltage floating (ISVF): +5,500 V.

Deconvolution, extraction, and visualization of the MS1 chromatogram of tryptic peptides were performed in Skyline software. Each peptide was quantified by merging intensities of one abundant precursor ion and its isotopes. Specifically, $[M+4H]^{4+}$ at *m/z* 741.6027 and *m/z* 761.5988 for the AMPK α 1-S347 peptide (DFYLATS³⁴⁷PPDSFLDDHHLTRPHER) and its singly phosphorylated form, respectively, and $[M+5H]^{5+}$ at *m/z* 809.1845 and *m/z* 825.1777 for the AMPK α 2-S345 peptide (IMNQASEFY-LASS³⁴⁵PPSGSFMDDSAMHIPGLKPHPER) and its singly phosphorylated form, respectively. As described previously (Steen et al., 2005), phosphorylation stoichiometry was measured by calculating the individual intensity of the phosphopeptide divided by the total intensity of the phosphopeptide plus its unmodified cognate.

Protein expression and purification from *Escherichia coli*

His₆-tagged AMPK was expressed in the *Escherichia coli* strain Rosetta (DE3) and grown in Luria-Bertani broth induced with 500 μ M isopropyl β -D-1-thiogalactopyranoside at 16°C before overnight incubation (Ngoei et al., 2018). Co-expression with N-myristoyl-transferase generated constructs N-terminally myristoylated on the Gly2 residue of the β -subunit. Cells were collected in ice-cold lysis buffer [50 mM Tris-HCl (pH 7.5), 500 mM NaCl, 5% glycerol, 50 mM imidazole, 10 μ M leupeptin, 0.1 mM AEBSF, 0.5 mM benzamidine-HCl and 2 mM BME] and lysed by a pre-cooled EmulsiFlex-C5 homogenizer (Avestin). Lysates were clarified by centrifugation (19,000 rpm, 60 min) and loaded onto a 5 mL nickel Sepharose column (HisTrapHP; GE Healthcare) and eluted with high-imidazole buffer [50 mM Tris-HCl (pH 7.5), 150 mM NaCl, 10% glycerol, 400 mM imidazole, 2 mM BME] and further purified by size-exclusion chromatography (SEC) in a buffer containing 50 mM Tris-HCl (pH 7.5), 150 mM NaCl, 10% glycerol and 2 mM TCEP. Pooled fractions were concentrated to \sim 1 mg/mL and flash-frozen in liquid nitrogen before storage at -80° C.

Protein expression for mammalian cell-based assays

Heterotrimeric AMPK was expressed in α dKO iMEFs. Human AMPK α 1 and α 2 (containing a C-terminal FLAG tag) was introduced into α 1^{-/-}/ α 2^{-/-} MEFs by lentiviral transduction using the LeGO iG2 system. Lentivirus-containing medium was replaced with an equal volume of fresh medium after 24 h. 72 h after transduction, MEFs were incubated with fresh medium for 1 h and treated as indicated. Heterotrimeric human AMPK (α 1 β 1 γ 1 and α 2 β 1 γ 1, expressed with an N-terminally GST-tagged α -subunit in pDEST27, C-terminally FLAG-tagged β 1-subunit in pcDNA3.1, and N-terminally HA-tagged γ 1-subunit in pMT2; wild-type or mutant protein as indicated) was expressed in HEK293T cells (Scott et al., 2014; Iseli et al., 2008). Cells at \sim 40–50% confluence were triply transfected with individual expression constructs for AMPK α -, β - and γ -subunits using the FuGENE HD transfection reagent according to the manufacturer's instructions. 48 h after transfection, the cells were incubated with fresh medium for 1 h and treated as indicated. All cells lines were harvested by initially washing with ice-cold PBS, then rapid *in situ* lysis with ice-cold lysis buffer [50 mM Tris-HCl (pH 7.4), 150 mM NaCl, 50 mM NaF, 1 mM sodium pyrophosphate, 1 mM EDTA, 1 mM EGTA, 1 mM DTT, 1% (vol/vol) Triton X-100 supplemented with protease inhibitors]. Lysates were clarified by centrifugation at 14,000 rpm for 5 min and flash-frozen in liquid nitrogen before storage at -80° C.

Axin co-immunoprecipitation

In accordance with a previously reported method (Zhang et al., 2018), α dKO iMEFs expressing either FLAG-tagged α 1 or α 2 were harvested as indicated above, but in ODG buffer [50 mM Tris-HCl (pH 8.0), 50 mM NaCl, 1 mM EDTA, 1 mM EGTA, 2% (vol/vol) octyl- β -D-glucopyranoside (ODG), 5 mM β -mercaptoethanol, supplemented with protease inhibitors]. Lysates were sonicated and then clarified by centrifugation at 20,000 \times *g* (4°C for 15 min). Supernatants containing AMPK complexes were immobilised on FLAG agarose resin for 3 h at 4°C followed by three washes in ODG buffer. After the final wash, the supernatant was removed, and beads were resuspended in SDS-PAGE sample buffer for subsequent immunoblot analysis.

Immunoblotting

Samples were separated by SDS–PAGE and transferred to Immobilon-FL PVDF membrane (EMD Millipore). Membranes were then blocked in PBS + 0.1% Tween-20 (PBST) with 2% non-fat milk for 1 h at room temperature and incubated at 4°C overnight with primary antibodies diluted in PBST. After sequential washes with PBST the following day, membranes were incubated with fluorescently labelled anti-rabbit or anti-mouse IgG secondary antibodies diluted in PBST with an IR680 or IR800 dye for 1 h at room temperature. Immunoreactive bands were visualized on an Odyssey Infrared Imaging System with densitometry analyses performed with ImageStudioLite software (LI-COR Biosciences).

AMPK activity assays

AMPK heterotrimers purified from cultured cells were immobilized on FLAG agarose and washed extensively with wash buffer [50 mM HEPES (pH 7.4), 150 mM NaCl, 10% glycerol, 1 mM DTT and 0.02% Tween-20] before kinase reactions were performed with radiolabelled [γ -³²P] ATP (Scott et al., 2008). Assays were conducted in the presence of 100 μ M of SAMS synthetic peptide substrate, 5 mM MgCl₂ and 200 μ M [γ -³²P]ATP for 10 min at 30°C on a shaking platform. Kinase reactions were terminated by spotting 15 μ L of the reaction mixture onto cation-exchange paper, which was then quenched in 1% phosphoric acid. Following an overnight wash in 1% phosphoric acid, ³²P transfer to the SAMS peptide was quantified by liquid scintillation counting using a TRI-CARB 4810TR 110 V liquid scintillation counter (PerkinElmer).

Phosphorylation assays

25 ng of active GSK3 α or mTORC1 was mixed with 250 ng of kinase-inactive bacterial expressed AMPK in 50 mM HEPES (pH 7.4), 150 mM NaCl, 10% glycerol, 0.01% Tween-20, 100 μ M ATP and 5 mM MgCl₂ for 30 min at 30°C without agitation. Reactions were terminated by spiking SDS-containing Laemmli sample buffer into the reaction mixture; 75 ng of AMPK was immunoblotted for detection of phosphorylation on α -S345/7 (GSK3 β and mTORC1) and α -T479 (GSK3 β only).

Lysosome immunoprecipitation

Lysosomes were enriched on HA-agarose adopting a modified version of a previously established protocol (Abu-Remaileh et al., 2017). MEFs stably expressing the integral lysosome membrane protein TMEM192, fused to a C-terminal 3xHA tag, were generated by lentiviral transduction and subsequent puromycin selection. Cells were incubated in fresh DMEM for 2 h and harvested in ice cold 136 mM KCl, 10 mM KH₂PO₄ (KPBS, adjusted to pH 7.2 with KOH) supplemented with protease inhibitors. Cells were pelleted by centrifugation (1,000 rpm, 2 min, 4°C), resuspended in KPBS + protease inhibitors (1 mL/10 cm dish), lysed in a Dounce homogenizer (70 strokes performed on ice) and intact cells removed by centrifugation as above. The resulting cell lysate (input) was incubated with 25 μ L anti-HA-affinity gel (pre-equilibrated with KPBS) on a rotating wheel for 10 min at 4°C and beads were washed once with 1 mL KPBS. Lysosomal proteins and contents were released from HA-agarose by addition of 75 μ L lysis buffer [50 mM Tris-HCl (pH 7.4), 150 mM NaCl, 50 mM NaF, 1 mM sodium pyrophosphate, 1 mM EDTA, 1 mM EGTA, 1 mM dithiothreitol, 1% (v/v) Triton X-100 plus protease inhibitors] for 10 min on ice.

Immunofluorescence and image analysis

HeLa cells were grown as monolayers on Poly-L-lysine-coated glass coverslips #1.5 (Proscitech) and triply transfected via FugeneHD with AMPK heterotrimers GFP- α 2 (WT or mutants as indicated), β 1-myc and HA- γ 1 [plasmid DNA ratio 1:2:1 (30:60:30 ng)] according to manufacturer's protocol. After 48 h, cells were treated \pm 50 nM torin1 for 1 h as indicated, fixed in 4% formaldehyde for 20 min, permeabilized in PBS with 1% BSA/0.2% Tween-20 for 20 min and blocked in 1% BSA in PBS for 1 h at room temperature. Glass coverslips were incubated with LAMP1 primary antibody overnight at 4°C. After successive washes with PBS, cells were incubated with Alexa Fluor 647 secondary antibody for 1 h in the dark at room temperature. Coverslips were mounted in Fluoroshield with DAPI mounting medium. Images were acquired at 20x magnification with a Nikon A1R Laser Scanning Confocal Microscope (BOMP, University of Melbourne). Images were collected sequentially for multicolor imaging: Alexa Fluor 647 was excited with a 638-nm red laser diode, GFP with the 488-nm line of an argon laser, and DAPI with a 405-nm UV laser. Detection parameters including "HV gain", "offset" and "laser power" were kept constant during image acquisition. Fluorescence images were contrast enhanced using Adobe Photoshop CS6 (Adobe), with specific care taken to ensure no loss of visual information. After defining the region of interest for each cell, the Pearson's correlation coefficient (PCC) (Manders et al., 1992) and Manders' co-localization coefficients (MCCs - MCC1: fraction of GFP signal co-localized with LAMP1 signal, MCC2: fraction of LAMP1 signal co-localized with GFP signal) (Manders et al., 1993) were calculated after thresholding, which represent statistical indicators for correlation and co-localization between the green (GFP) and red (Alexa Fluor 647) fluorescent channels, respectively.

Live cell imaging

HeLa cells were seeded at 1.8×10^5 cells/well in 170 μ L 35 \times 10 mm cell imaging dishes (Eppendorf) for 24 h prior to transfection. Cells were triply transfected with AMPK heterotrimers GFP- α 2/myc- β 1/HA- γ 1 (plasmid DNA ratio 1:2:1; 30:60:30 ng) and 12 μ L lipofectamine2000 in 300 μ L OPTI-MEM 1 (Gibco) per well. 24 h post transfection, media was replaced with fresh DMEM media for another 24 h before imaging. Lysosomal regions of cells transfected with AMPK- α 2(S345/S345A/S345E), β 1 and γ 1 plasmids

were identified by endocytic staining with 5 $\mu\text{g}/\text{mL}$ FM4-64. These cells were imaged on an Eclipse TE2000-E microscope (Nikon) with a Cascade II 1024 camera using software Metamorph V7.7.9.0 (Molecular Devices, LLC).

Fluorescence recovery after photobleaching (FRAP) of mammalian cells

HeLa cells were seeded at 1.8×10^5 cells/well in 170 μL 35 \times 10 mm cell imaging dishes (Eppendorf) for 24 h prior to transfection. Cells were triply transfected via Lipofectamine 2000 with heterotrimeric AMPK comprising GFP- $\alpha 2$, myc- $\beta 1$ and HA- $\gamma 1$ [plasmid DNA ratio 1:2:1 (30:60:30 ng)] according to the manufacturer's protocol. 24 h post transfection, and 40 min prior to imaging, 2.5 $\mu\text{g}/\text{mL}$ nocodazole (Sigma) was added to the cell media to reduce lysosomal movement and the plates returned to the CO_2 incubator. Cells were imaged on an Eclipse TE2000-E microscope (Nikon) with a Cascade II 1024 camera. FRAP was performed on cells on a Leica TCS SP5 Laser Scanning Confocal Microscope with a 30°C heated stage, using a HPX Plan Apo 60x water immersion lens. Images were acquired using a 488 nm argon laser at 4x zoom with a confocal pinhole size set to 5 Airy units and detected with a PMT2 detector set from 500–600 nm (1093 gain, 0 offset). For FRAP analysis, pre-bleached images were taken using 1% laser power, selected lysosomal regions were bleached at 25% laser power, followed by successive post-bleached images taken using 1% laser power for up to 3 min.

Cell proliferation analysis

MEFs isolated from WT or $\alpha 2$ -S345A whole-body KI mice were seeded at approximately 10–15%. After 24 h, media was replaced with fresh, arginine/lysine/leucine free DMEM [supplemented with 10% FBS, 4 mM L-glutamine, 3.7 g/L sodium bicarbonate, 0.8 mM lysine and penicillin-streptomycin, with or without 0.8 mM leucine and/or 0.4 mM arginine]. Cell proliferation was then analysed in real-time by the Incucyte® Live-Cell Analysis System according to the manufacturer's instructions.

QUANTIFICATION AND STATISTICAL ANALYSIS

Statistical significance is indicated in the figure legends. Statistics were performed using Prism (GraphPad) 7 software. Immunofluorescence images were obtained using NIS Elements software (Nikon Instruments Inc.) and analysed using Volocity 6.3 (Perkin Elmer) imaging software. FRAP images were obtained using Metamorph V7.7.9.0 software (Molecular Devices, LLC) and analysed using LASAF (Leica Applications Suite Advanced Fluorescence) software within the LASAF FRAP wizard. Immunoblots were analysed using ImageJ (NIH). Results from replicate experiments (n) were expressed as means \pm standard deviation (s.d.) or standard error (s.e.m.). All measurements were taken from distinct samples. All statistical tests were performed using one- or two-way analysis of variance (ANOVA) with Dunnett's multiple comparisons test or unpaired, two-tailed Student's *t* test.